TECHNICAL REPORT No. 28

AN ENERGY AND ANGULAR MOMENTUM CONSERVING FINITE-DIFFERENCE SCHEME, HYBRID COORDINATES AND MEDIUM-RANGE WEATHER PREDICTION

by

A. J. Simmons and R. Strüfing

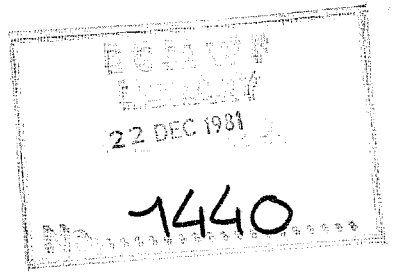

November 1981

C O N T E N T S

		PAGE
ABSTRACT		1
1.	INTRODUCTION	1
2.	CONTINUOUS FORMULATION	1
3.	AN ENERGY AND ANGULAR MOMENTUM CONSERVING VERTICAL FINITE-DIFFERENCE SCHEME	4
3.1	Distribution of levels	5
3.2	Continuity equation	5
3.3	Vertical advection	5
3.4	Hydrostatic equation and pressure-gradient term	6
3.5	Energy conversion term	8
3.6	Horizontal representation of the pressure gradient	8
3.7	Full-level values of pressure	10
4.	GRAVITY WAVES AND A SEMI-IMPLICIT TIME SCHEME	11
5.	VERTICAL COORDINATES	12
6.	VERTICAL RESOLUTIONS	15
7.	CANCELLATION OF GEOPOTENTIAL AND PRESSURE GRADIENT TERMS OVER STEEP OROGRAPHY	19
8.	STABILITY OF THE SEMI-IMPLICIT TIME SCHEME	24
9.	REPRESENTATION OF FORCED PLANETARY-WAVE MOTION	28
10.	IMPLEMENTATION IN THE ECMWF GRID-POINT FORECAST MODEL	31
11.	FORECAST CASES	32
12.	FORECAST RESULTS	33
12.1	Objective verification	33
12.2	Synoptic assessment	40
12.3	Stratospheric forecasts	44
12.4	The traditional hybrid coordinate	53
12.5	Other results	57
13.	CONCLUDING REMARKS	57
REFERENCES		60
APPENDIX A	THE CONSERVATION OF ANGULAR MOMENTUM	62
APPENDIX B	MATRICES AND VECTORS FOR THE SEMI-IMPLICIT SCHEME	64
APPENDIC C	SOME DETAILS OF THE FORMULATION OF THE QUASI-GEOSTROPHIC MODEL	65

ABSTRACT

An energy and angular-momentum conserving vertical finite-difference scheme is introduced for a general terrain-following vertical coordinate which is a function of pressure and its surface value. A corresponding semi-implicit time scheme is also defined.

These schemes are first used to compare some idealized properties of the usual sigma coordinate with those of the hybrid coordinate which reduces to pressure above a fixed level and also with those of alternative hybrid coordinates which tend uniformly to pressure at upper levels. Error in the representation of the stratospheric pressure gradient over steep orography can be significantly reduced by use of the traditional hybrid coordinate, but the semi-implicit scheme is less stable. The alternative hybrid coordinates offer a useful compromise. Sigma- and hybrid- coordinate results for steady, forced, planetary-wave structures can be significantly different when the upper-level resolution is inadequate.

The implementation of these schemes and coordinates in the ECMWF grid-point forecast model is briefly described and results are presented for four situations. Forecasts are shown to be generally insensitive to the choice of vertical coordinate but those differences that are found are mostly such as to favour choice of one of the alternative hybrid coordinates. Remarkably accurate stratospheric forecasts of sudden warming events using models with topmost levels at either 25mb or 10mb are also illustrated. Practical experience confirms the results of the idealized analysis of the stability of the semi-implicit scheme.

1. INTRODUCTION

The use of sigma, pressure divided by its surface value, as the vertical coordinate in a primitive equation model (Phillips, 1957) produces a system of equations with a much simpler lower boundary condition than in a pressure-coordinate model, but this simplicity is obtained at the expense of introducing other difficulties. Over steep orography care has to be taken to ensure the correct degree of cancellation between the two components which comprise the pressure gradient in the momentum equation, and difficulties may arise if "horizontal" diffusion is applied along sigma surfaces. Results must be interpolated to pressure levels for purposes of presentation, general archiving and comparison with other model or observational studies, and energetics calculations using pressure-level output may not reproduce exact model balances.

Some of these difficulties become particularly apparent in models designed largely for stratospheric simulation, and to circumvent them, use has been made of a hybrid vertical coordinate suggested by Sangster (1960) which is similar to the usual sigma coordinate at low levels, but which reduces to pressure above a certain fixed level(Arakawa and Lamb,1977; Schlesinger and Mintz, 1979; Fels et al., 1980).

A further difficulty with a sigma-coordinate model arises in the context of numerical weather prediction if, as in the first operational system at ECMWF, the data analysis is carried out on pressure levels. To provide sigma-level data over high ground, such an analysis must be carried out at a higher level than is required to provide data at the height of the sigma-level over the oceans. A model field must thus be both interpolated and extrapolated to provide a first-guess pressure-level field for input to the analysis, and interpolation of the resulting pressure coordinate analysis back to sigma coordinates is also required. Problems again become marked at stratosperic levels where model resolution is coarse.

The purpose of the present report is three-fold. Firstly, in the following three sections we set down the form of the continuous primitive equations for a general pressure-based terrain-following vertical coordinate, following Kasahara (1974), and present a vertical finite-difference formulation of these equations which conserves both energy and angular momentum. We include also a formulation of a corresponding semi-implicit time scheme.

These formulations are then used to compare some of the idealized properties of different vertical coordinates. Two of these are the traditional sigma coordinate and the usual hybrid coordinate which reduces to pressure above a certain level. The latter exhibits a number of advantages over the sigma coordinate, but has the disadvantage of a marked irregularity in the distribution of layer thicknesses over high ground. We thus also investigate hybrid vertical coordinates for which the transition towards a pure pressure coordinate occurs smoothly as the pressure decreases towards zero.

The properties of the different vertical coordinates are examined in three respects. We first follow a number of authors, among them Corby et al (1972), Gary (1973), Sundgvist (1976), Nakamura (1978) and Mesinger (1981), in examining the error in the representation of the pressure gradient over steep orography. Secondly, we examine the stability of the semi-implicit time scheme as analyzed for a sigma-coordinate model by Simmons et al (1978). We then compare the representation of forced planetary-scale motion in a steady, quasi-geostrophic model.

The third aspect of this study concerns the behaviour of the alternative vertical coordinates in numerical weather prediction. The implementation of the general vertical finite-difference scheme in the grid-point model developed for operational forecasting at ECMWF is briefly described, and the performance of sigma and hybrid coordinates is compared for 10 day forecasts. The four cases chosen for study include examples of marked stratospheric warmings and the simulation of these is illustrated. Hybrid forecasts are presented for resolutions with top levels at 25 and 10 mb respectively.

2. CONTINUOUS FORMULATION

We consider a general, terrain-following, vertical coordinate η, a monotonic function of pressure, p, and dependent on its surface value p_s:

$$\eta = h(p,p_s)$$

where $h(0,p_s) = 0$ and $h(p_s,p_s) = 1$

The continuous formulation of the primitive equations may be directly written down following Kasahara (1974).

The momentum and thermodynamic equations for frictionless adiabatic motion are

$$\frac{D\underset{\sim}{v}}{Dt} + f\underset{\sim}{k} \times \underset{\sim}{v} + \nabla\Phi + \frac{RT}{p}\nabla p = 0 \qquad (2.1)$$

and

$$\frac{DT}{Dt} - \frac{\kappa T\omega}{p} = 0 \qquad (2.2)$$

The continuity equation may be written

$$\frac{\partial}{\partial\eta}\left(\frac{\partial p}{\partial t}\right) + \nabla.\left(\underset{\sim}{v}\frac{\partial p}{\partial\eta}\right) + \frac{\partial}{\partial\eta}\left(\dot{\eta}\frac{\partial p}{\partial\eta}\right) = 0 \qquad (2.3)$$

while the hydrostatic equation is

$$\frac{\partial\Phi}{\partial\eta} = -\frac{RT}{p}\frac{\partial p}{\partial\eta} \qquad (2.4)$$

Here t is time and $\frac{D}{Dt}$ is the material derivative, which in η-coordinates takes the form

$$\frac{\partial}{\partial t} + u\frac{\partial}{\partial x} + v\frac{\partial}{\partial y} + \dot{\eta}\frac{\partial}{\partial \eta}$$

for a cartesian coordinate system with x eastward and y northward, and eastward and northward velocity components u and v. $\underset{\sim}{v}$ is the horizontal velocity vector, $\underset{\sim}{v} = (u,v,0)$, and ∇ the horizontal gradient operator: $\nabla \equiv (\frac{\partial}{\partial x}, \frac{\partial}{\partial y}, 0)$ for the cartesian system. f is the Coriolis parameter, $\underset{\sim}{k}$ the unit vertical vector, Φ the geopotential, T the temperature, R the gas constant, and $\kappa = R/c_p$, where c_p is the specific heat at constant pressure. ω is given by

$$\omega \equiv \frac{Dp}{Dt} = -\int_o^\eta \nabla \cdot (\underset{\sim}{v}\frac{\partial p}{\partial \eta})\, d\eta + \underset{\sim}{v}\cdot\nabla p \qquad (2.5)$$

Explicit expressions for the rate of change of surface pressure, and for $\dot{\eta}$, are obtained by integrating (2.3) using the boundary conditions $\dot{\eta} = 0$ at $\eta = 0$ and $\eta = 1$:

$$\frac{\partial p_s}{\partial t} = -\int_o^1 \nabla \cdot (\underset{\sim}{v}\frac{\partial p}{\partial \eta})\, d\eta \qquad (2.6)$$

and

$$\dot{\eta}\frac{\partial p}{\partial \eta} = -\frac{\partial p}{\partial t} - \int_o^\eta \nabla \cdot (\underset{\sim}{v}\frac{\partial p}{\partial \eta})\, d\eta \qquad (2.7)$$

3. AN ENERGY AND ANGULAR MOMENTUM CONSERVING VERTICAL FINITE-DIFFERENCE SCHEME

A feature of the vertical finite-difference scheme described in this section is its generality. The vertical coordinate appears only implicitly, through values of pressure, p, and its derivative with respect to surface pressure, $\partial p/\partial p_s$, at each of the model levels. The scheme itself has elements in common with a number of sigma-coordinate schemes, in particular that used in the ECMWF grid-point and spectral models (Burridge and Haseler, 1977). It differs from the latter in that the calculation of geopotential is modified to ensure conservation of angular momentum.

3.1 Distribution of levels

Prognostic variables u, v and T (and more generally the moisture variable also) are carried at in general unequally-spaced "full" levels k = 1,2,.....NLEV, and we define values of the vertical coordinate, $\eta_{k+\frac{1}{2}}$, and thus the pressure $p_{k+\frac{1}{2}}$ and its gradient $(\partial p/\partial p_s)_{k+\frac{1}{2}}$ at intermediate "half" levels. The pressure difference between half levels is given by

$$\Delta p_k = p_{k+\frac{1}{2}} - p_{k-\frac{1}{2}} \tag{3.1}$$

3.2 Continuity equation

The natural finite-difference analogue of (2.6) is

$$\frac{\partial p_s}{\partial t} = - \sum_{r=1}^{NLEV} \nabla . (\underset{\sim}{v}_r \Delta p_r) \tag{3.2}$$

while (2.7) yields half-level values of $\dot{\eta} \frac{\partial p}{\partial \eta}$:

$$(\dot{\eta} \frac{\partial p}{\partial \eta})_{k+\frac{1}{2}} = - \frac{\partial p_{k+\frac{1}{2}}}{\partial t} - \sum_{r=1}^{k} \nabla . (\underset{\sim}{v}_r \Delta p_r)$$

This may be written, using (3.2),

$$(\dot{\eta} \frac{\partial p}{\partial \eta})_{k+\frac{1}{2}} = (\frac{\partial p}{\partial p_s})_{k+\frac{1}{2}} \sum_{r=1}^{NLEV} \nabla . (\underset{\sim}{v}_r \Delta p_r) - \sum_{r=1}^{k} \nabla . (\underset{\sim}{v}_r \Delta p_r) \tag{3.3}$$

3.3 Vertical advection

Conservation of energy is preserved by the vertical advection terms if the advection of a variable F is such as to satisfy the finite-difference analogues of the relations

$$\int_0^1 \dot{\eta} \frac{\partial F}{\partial \eta} \frac{\partial p}{\partial \eta} \, d\eta = - \int_0^1 F \frac{\partial}{\partial \eta} (\dot{\eta} \frac{\partial p}{\partial \eta}) \, d\eta$$

and

$$\int_0^1 \dot{\eta} F \frac{\partial F}{\partial \eta} \frac{\partial p}{\partial \eta} \, d\eta = - \int_0^1 \tfrac{1}{2} F^2 \frac{\partial}{\partial \eta} (\dot{\eta} \frac{\partial p}{\partial \eta}) \, d\eta$$

This is achieved by choosing

$$(\dot{\eta}\,\frac{\partial F}{\partial \eta})_k = \frac{1}{2\Delta p_k}\,\{(\dot{\eta}\,\frac{\partial p}{\partial \eta})_{k+\frac{1}{2}}\,(F_{k+1}-F_k) + (\dot{\eta}\frac{\partial p}{\partial \eta})_{k-\frac{1}{2}}\,(F_k-F_{k-1})\} \qquad (3.4)$$

In the examples given in later sections, this form is used for T as well as u and v. Arakawa and Lamb (1977) describe an alternative differencing for temperature in order to conserve $\ln\theta$, where θ is potential temperature.

3.4 Hydrostatic equation and pressure-gradient term

The form chosen for the finite-difference analogue of the hydrostatic equation (2.4) is

$$\Phi_{k+\frac{1}{2}} - \Phi_{k-\frac{1}{2}} = -\,RT_k\,\ln\frac{p_{k+\frac{1}{2}}}{p_{k-\frac{1}{2}}}$$

giving

$$\Phi_{k+\frac{1}{2}} = \Phi_s + \sum_{r=k+1}^{NLEV} RT_r\,\ln\frac{p_{r+\frac{1}{2}}}{p_{r-\frac{1}{2}}} \qquad (3.5)$$

where $\Phi_{k+\frac{1}{2}}$ is a half-level value, Φ_s the surface value, and we adopt the convention

$$\sum_{r=NLEV+1}^{NLEV}(\quad) \equiv 0$$

When used in the momentum equations full level values of Φ are required and, for the moment, we write simply

$$\Phi_k = \Phi_{k+\frac{1}{2}} + \alpha_k\,RT_k \qquad (3.6)$$

It is not, in fact, necessary to specify α_k in order to ensure conservation of energy and angular momentum, and values may be chosen to enhance the accuracy of the scheme. A specific choice is made at the end of this sub-section.

Intimately connected with the form chosen for the integration of the hydrostatic equation is the expression for full level values of the pressure gradient term $(RT/p)\nabla p$ in terms of the known half-level values $p_{k+\frac{1}{2}}$ and $\nabla p_{k+\frac{1}{2}}$. We determine this expression by requiring that the vertical difference scheme preserves the conservation of angular momentum:

$$\int_0^{2\pi} \{ \int_0^1 (\frac{\partial \Phi}{\partial \lambda} + \frac{RT}{p} \frac{\partial p}{\partial \lambda}) (\frac{\partial p}{\partial \eta}) d\eta + \Phi_s \frac{\partial p_s}{\partial \lambda} \} d\lambda = 0$$

where λ is longitude. This requires, in finite difference form,

$$\sum_{r=1}^{NLEV} \Phi_r \frac{\partial}{\partial \lambda} \Delta p_r = \Phi_s \frac{\partial p_s}{\partial \lambda} + \sum_{r=1}^{NLEV} R(\frac{T}{p} \frac{\partial p}{\partial \lambda})_r \Delta p_r \qquad (3.7)$$

which is satisfied if

$$(\frac{RT}{p} \nabla p)_k = \frac{RT_k}{\Delta p_k} \{ (\ln \frac{p_{k+\frac{1}{2}}}{p_{k-\frac{1}{2}}}) \nabla p_{k-\frac{1}{2}} + \alpha_k \nabla (\Delta p_k) \} \qquad (3.8)$$

Further detail is given in Appendix A.

Angular momentum conservation is hereby achieved without the artificial dependence of geopotential on the temperature of all model levels that occurs in the scheme described by Arakawa and Lamb (1977). This is a consequence of using half-level values of Φ in the summation (3.5) of the hydrostatic equation.

The value of α_k in (3.6) and (3.8) must be specified in any application of the scheme outlined here. One choice could be to require cancellation of error in the sum of the geopotential and pressure gradient terms for a reference temperature distribution which is a function of pressure alone. Here we restrict attention to an alternative which causes (3.8) to reduce to the usual form

$$RT_k \nabla \ln p_s$$

for a sigma-coordinate model. This is achieved if

$$\alpha_k = 1 - \frac{p_{k-\frac{1}{2}}}{\Delta p_k} \ln \frac{p_{k+\frac{1}{2}}}{p_{k-\frac{1}{2}}} \qquad (3.9)$$

and in this case (3.8) may be written

$$(\frac{RT}{p} \nabla p)_k = RT_k \nabla \{ \frac{1}{\Delta p_k} (p_{k+\frac{1}{2}} \ln p_{k+\frac{1}{2}} - p_{k-\frac{1}{2}} \ln p_{k-\frac{1}{2}}) \} \qquad (3.10)$$

The right-hand side of this expression may be viewed as a finite difference approximation to $RT \nabla(\frac{\partial}{\partial p} (p \ln p))$, $= RT \nabla \ln p$.

3.5 Energy conversion term

To obtain a form for the term $\frac{\kappa T\omega}{p}$ in (2.2) we use (2.5) to write

$$\frac{\kappa T\omega}{p} = -\frac{\kappa T}{p}\int_0^{\eta} \nabla.(\underset{\sim}{v}\frac{\partial p}{\partial \eta})\, d\eta + \kappa T\,\underset{\sim}{v}.\,(\frac{1}{p}\nabla p) \tag{3.11}$$

Full-level values of this expression are then determined by the requirement that the difference scheme conserves the total energy of the model atmosphere for adiabatic, frictionless motion. This is achieved by generalizing the sigma-coordinate scheme described by Burridge and Haseler (1977) such that

(i) the first term on the right-hand side of (3.11) is evaluated at level k by

$$-\frac{\kappa T_k}{\Delta p_k}\{(\ell n\,\frac{p_{k+\frac{1}{2}}}{p_{k-\frac{1}{2}}})\sum_{r=1}^{k-1}\nabla.(\underset{\sim}{v}_r\,\Delta p_r) + \alpha_k\nabla.(\underset{\sim}{v}_k\,\Delta p_k)\} \tag{3.12}$$

(ii) the second term is evaluated as

$$\kappa T_k\,\underset{\sim}{v}_k.\,(\frac{1}{p}\nabla p)_k \tag{3.13}$$

where the term $(\frac{1}{p}\nabla p)_k$ is calculated in the same way as in the momentum equation.

3.6 Horizontal representation of the pressure gradient

In a model with a finite-difference representation in the horizontal, two alternative forms for the pressure gradient are suggested by equations (3.8) and (3.10). We illustrate these for a grid for which values of surface pressure (and thus pressure) and temperature are defined at the same point, and consider explicitly only the zonal derivative. We first define the usual operators

$$\delta_\lambda A = \{A(\lambda + \Delta\lambda/2) - A(\lambda - \Delta\lambda/2)\} / \Delta\lambda$$

and

$$\overline{A}^\lambda = \tfrac{1}{2}\{A(\lambda + \Delta\lambda/2) + A(\lambda - \Delta\lambda/2)\}$$

If the geopotential gradient is represented by

$$\frac{1}{a \cos\theta}\,\delta_\lambda \phi_k$$

where θ is latitude and a the radius of the earth, the appropriate form of the pressure gradient for conservation of angular momentum is derived from (3.8) and is

$$\frac{R}{a \cos\theta \overline{\Delta p_k}^\lambda}\left\{\overline{(T_k(\ln\frac{p_{k+\frac{1}{2}}}{p_{k-\frac{1}{2}}})}^\lambda \delta_\lambda p_{k-\frac{1}{2}} + \overline{(\alpha_k T_k)}^\lambda \delta_\lambda \Delta p_k\right\} \qquad (3.14)$$

provided the geopotential and pressure gradient terms are multiplied by $\overline{\Delta p_k}^\lambda$ in the expression for the rate of change of angular momentum.

An alternative representation of the pressure gradient term is derived directly from (3.10):

$$\frac{R\overline{T}^\lambda}{a \cos\theta}\,\delta_\lambda\left\{\frac{1}{\Delta p_k}(p_{k+\frac{1}{2}}\ell n p_{k+\frac{1}{2}} - p_{k-\frac{1}{2}}\ell n p_{k-\frac{1}{2}})\right\} \qquad (3.15)$$

This is direct generalization of the σ-coordinate form

$$\frac{R\overline{T}^\lambda}{a \cos\theta}\,\delta_\lambda \ell n p_s$$

discussed by Corby et al. (1972). For the present vertical scheme (3.15) implies exact cancellation of the geopotential and pressure gradient terms for a temperature profile of the form $T = A\ell n p + B$ for finite $\Delta\lambda$ in the limit as $\Delta p_k \to 0$, and for finite Δp_k in a sigma coordinate model if full level pressures are appropriately defined, as demonstrated in section 7.

Precise implementation of the vertical finite-difference scheme described above in a spectral model would require calculation of additional spectral/grid -point transforms associated with the computation of pressure gradients. However, the relationship

$$\nabla p_{k+\frac{1}{2}} = p_s \left(\frac{\partial p}{\partial p_s}\right)_{k+\frac{1}{2}} \nabla \ell n p_s \qquad (3.16)$$

may be used to avoid such transforms.

3.7 Full-level values of pressure

A feature of the finite difference scheme described here is that no reference is made to full-level values of the vertical coordinate, or equivalently pressure. Such full-level values are required, however, for the determination of initial values of prognostic variables, and more generally, as input to parameterization schemes.

Two different full-level values of p are suggested by the finite-difference scheme. (3.12) is an approximation to a term

$$-\frac{\kappa T}{p}\int_0^{\eta} \nabla\cdot\left(\underset{\sim}{v}\frac{\partial p}{\partial \eta}\right) d\eta$$

and may generally be written

$$-\frac{\kappa T_k}{\Delta p_k}\,\ell n\,\frac{p_{k+\frac{1}{2}}}{p_{k-\frac{1}{2}}}\left\{\sum_{r=1}^{k-1}\nabla\cdot\left(\underset{\sim}{v}_r\,\Delta p_r\right)+\left[\frac{1}{2}+o\left(\frac{\Delta p_k}{p_{k-\frac{1}{2}}}\right)\right]\nabla\cdot\left(\underset{\sim}{v}_k\,\Delta p_k\right)\right\}$$

For k = 1 the simplest equivalent is

$$-\frac{\kappa T_1}{(\Delta p_1/2)}\left\{\frac{1}{2}\nabla\cdot\left(\underset{\sim}{v}_1\,\Delta p_1\right)\right\}$$

These expressions suggest the full-level values

$$\left.\begin{aligned} p_k &= \frac{\Delta p_k}{\ell n\left(p_{k+\frac{1}{2}}/p_{k-\frac{1}{2}}\right)} \quad , \quad k>1 \\ p_1 &= \tfrac{1}{2}\Delta p_1 \end{aligned}\right\} \tag{3.17}$$

From (3.10) we obtain an alternative

$$p_k = \exp\left\{\frac{1}{\Delta p_k}\left(p_{k+\frac{1}{2}}\,\ell n p_{k+\frac{1}{2}} - p_{k-\frac{1}{2}}\,\ell n p_{k-\frac{1}{2}}\right) - C\right\} \tag{3.18}$$

where C is independent of the horizontal coordinates.
Setting C = 1 yields an appropriate P_k in the limit $\Delta p_k/p_{k-\frac{1}{2}} \to 0$
and also a full-level value for P_1 which is consistent with the hydrostatic equation (see (3.6) and (3.9)) for an isothermal atmosphere.

Away from the upper boundary (3.17) and (3.18) both yield

$$p_k = \frac{1}{2}\left(p_{k+\frac{1}{2}} + p_{k-\frac{1}{2}}\right) + o\left\{(\Delta p_k)^2 / p_{k-\frac{1}{2}}\right\} ,$$

but top level values are given by $\Delta p_1 /2$ and $\Delta p_1/e$ respectively. This ambiguity may be resolved at the possible expense of angular momentum conservation by using the value $\alpha_1 = \ell n2$ in (3.6) and (3.12). In this case

$$\phi_1 = \phi_{1\frac{1}{2}} + (\ell n2)\ RT_1 \tag{3.19}$$

and C in (3.18) should take the value 1 at all but the top level, where $C = \ell n2$. Loss of angular momentum conservation will not occur if the uppermost coordinate surfaces are surfaces of constant pressure.

We return to this point with specific examples in later sections.

4. GRAVITY WAVES AND A SEMI-IMPLICIT TIME SCHEME

We here follow the development given for a sigma-coordinate model by Hoskins and Simmons (1975). For the more general coordinate it is necessary to introduce not only a reference temperature profile, but also a reference value for the surface pressure. Variables defined at each of the NLEV levels of the model are represented by columns vectors, and we denote the reference temperature profile by $\underset{\sim}{T}_r$ and the reference pressure by p_r.

Linearizing about the resting basic state $(\underset{\sim}{T}_r, p_r)$, the divergence, temperature, surface pressure and hydrostatic equations may be written

$$\frac{\partial \underset{\sim}{D}}{\partial t} = \underset{\sim}{D} - \nabla^2\{\underset{\sim}{\phi} + \underset{\sim}{h}_1 p'_s\} \tag{4.1}$$

$$\frac{\partial \underset{\sim}{T}'}{\partial t} = \underset{\sim}{T} - \underset{\sim\sim}{\tau} \underset{\sim}{D} \tag{4.2}$$

$$\frac{\partial p'_s}{\partial t} = \underset{\sim}{P} - \underset{\sim}{\nu}\cdot \underset{\sim}{D} \tag{4.3}$$

and

$$\phi = \underset{\sim}{H} + \underset{\sim\sim}{\gamma} \underset{\sim}{T}' + \underset{\sim}{h}_2 p'_s \tag{4.4}$$

Here $\underset{\sim}{D}$ is the divergence, $\underset{\sim}{T}' = \underset{\sim}{T} - \underset{\sim}{T}_r$, $p'_s = p_s - p_r$, and $\underset{\sim}{D}$, $\underset{\sim}{T}$, $\underset{\sim}{P}$ and $\underset{\sim}{H}$ contain all nonlinear terms. The constant matrices and vectors $\underset{\sim\sim}{\gamma}$, $\underset{\sim\sim}{\tau}$, $\underset{\sim}{h}_1$, $\underset{\sim}{h}_2$ and $\underset{\sim}{\nu}$ are defined in Appendix B for the vertical scheme described in the preceding section.

Neglecting the nonlinear terms leads to the following gravity-wave equation

$$\frac{\partial^2 \underset{\sim}{D}}{\partial t^2} = \nabla^2 \underset{\sim\sim}{B}\ \underset{\sim}{D}$$

where

$$\underset{\approx}{B} = \underset{\approx}{\gamma}\,\underset{\approx}{\tau} + (\underset{\sim}{h}_1 + \underset{\sim}{h}_2).\underset{\sim}{\nu} \qquad (4.5)$$

The eigenvalues of $\underset{\sim}{B}$ are the squares of the gravity-wave phase speeds, and examples are presented in section 8.

Equations (4.1) to (4.4) may readily be used to define a semi-implicit time scheme. Just as in a sigma-coordinate model, the nonlinear terms $\underset{\sim}{D}$, $\underset{\sim}{T}$, $\underset{\sim}{P}$ and $\underset{\sim}{H}$ are evaluated at time t, while the linear terms on the right-hand sides are evaluated as the arithmetic mean of values at time $t + \Delta t$ and $t - \Delta t$. The largest difference from a sigma-coordinate scheme is the more complicated form of the hydrostatic equation, which includes a term to be evaluated explicitly.

Simmons et al. (1978) demonstrated that the reference temperature profile $\underset{\sim}{T}_r$ must be carefully chosen to avoid computational instability in a sigma coordinate model. More generally, similar considerations apply to the choice of the reference surface pressure. Specific examples are discussed in section 8.

5. VERTICAL COORDINATES

We examine the performance of the difference schemes outlined in the preceding sections for four vertical coordinates. The first is the usual sigma coordinate (Phillips, 1957) for which

$$p_{k+\frac{1}{2}} = p_s \;\eta_{k+\frac{1}{2}} \qquad \text{and} \quad (\partial p/\partial p_s)_{k+\frac{1}{2}} = \eta_{k+\frac{1}{2}}.$$

The second coordinate, which will be referred to as coordinate type 2, is in essence the hybrid coordinate described by Arakawa and Lamb (1977). For this coordinate we define an inter-facial pressure $p_{I+\frac{1}{2}}$ with corresponding half-level value $\eta_{I+\frac{1}{2}}$

Then

$$p_{k+\frac{1}{2}} = p_{I+\frac{1}{2}}\,\eta_{k+\frac{1}{2}}/\,\eta_{I+\frac{1}{2}} \qquad \text{for} \quad \eta_{k+\frac{1}{2}} \leq \eta_{I+\frac{1}{2}},$$

and

$$p_{k+\frac{1}{2}} = p_{I+\frac{1}{2}} + (\,\eta_{k+\frac{1}{2}} - \eta_{I+\frac{1}{2}})\;(p_s - p_{I+\frac{1}{2}})/(1-\eta_{I+\frac{1}{2}}) \qquad \text{otherwise,}$$

with

$$\left(\frac{\partial p}{\partial p_s}\right)_{k+\frac{1}{2}} = 0 \quad \text{for } \eta_{k+\frac{1}{2}} \leq \eta_{I+\frac{1}{2}},$$

$$= (\,\eta_{k+\frac{1}{2}} - \eta_{I+\frac{1}{2}})/(1-\eta_{I+\frac{1}{2}}) \text{ otherwise.}$$

The third vertical coordinate (coordinate 3) is designed to have smoothly varying layer thicknesses, but to tend to a pressure coordinate at upper levels. In continuous form we define

$$\eta = \frac{p}{p_s} + \left(\frac{p}{p_s} - 1\right)\left(\frac{p}{p_s} - \frac{p}{p_o}\right), \qquad p_o \text{ a constant.}$$

Then $\eta=1$ when $p=p_s$ and $\eta \sim p/p_o$ as $p \to 0$. η varies monotonically from $p = p_s$ to $p = 0$ provided $p_o > \frac{1}{2}\,\mathrm{Max}(p_s)$. In the following examples we choose $p_o = 1013.2$ mb. In this case the pressure on a coordinate surface varies by about 1% near the 10mb level as the surface pressure varies in the range $1013\text{mb} > p_s > 500\text{mb}$. Half-level values are given by

$$p_{k+\frac{1}{2}} = \frac{2p_o\,\eta_{k+\frac{1}{2}}}{\left(1+\sqrt{1+4\eta_{k+\frac{1}{2}}\,p_o(p_o-p_s)/p_s^2}\right)}$$

and

$$\left(\frac{\partial p}{\partial p_s}\right)_{k+\frac{1}{2}} = \frac{p_{k+\frac{1}{2}}\left(p_{k+\frac{1}{2}}/p_s\right)^2\left(2p_o/p_s - 1\right)}{\left(2\,\eta_{k+\frac{1}{2}}\,p_o - p_{k+\frac{1}{2}}\right)}.$$

Coordinate 4 is one of a class of coordinates (which includes the sigma coordinate and hybrid coordinate type 2) defined implicitly by the relation

$$p_{k+\frac{1}{2}} = A_{k+\frac{1}{2}}\,p_o + B_{k+\frac{1}{2}}\,p_s \qquad (5.1)$$

with $\left(\frac{\partial p}{\partial p_s}\right)_{k+\frac{1}{2}} = B_{k+\frac{1}{2}}$. Here p_o is a constant pressure, again taken to be 1013.2 mb, and the $A_{k+\frac{1}{2}}$ and $B_{k+\frac{1}{2}}$ are constants. Values of the A's and B's are chosen to give coordinate surfaces which tend, as pressure decreases, to surfaces of constant pressure more rapidly than for coordinate 3. Their precise specification is resolution dependent and given in the following section.

The form of coordinate given by (5.1) is particularly efficient from a computational viewpoint, and allows a direct control over the "flattening" of coordinate surfaces as the pressure decreases, since the A's and B's may be determined by specifying the distribution of model pressure levels for a mean sea-level pressure and for a surface pressure typical of the lowest expected to be attained in the model. The more complicated form of coordinate 3 is included here since it was used for a number of forecast experiments prior to the introduction of coordinate 4; a coordinate very similar to it may be obtained from (5.1) by an appropriate choice of the $A_{k+\frac{1}{2}}$ and $B_{k+\frac{1}{2}}$.

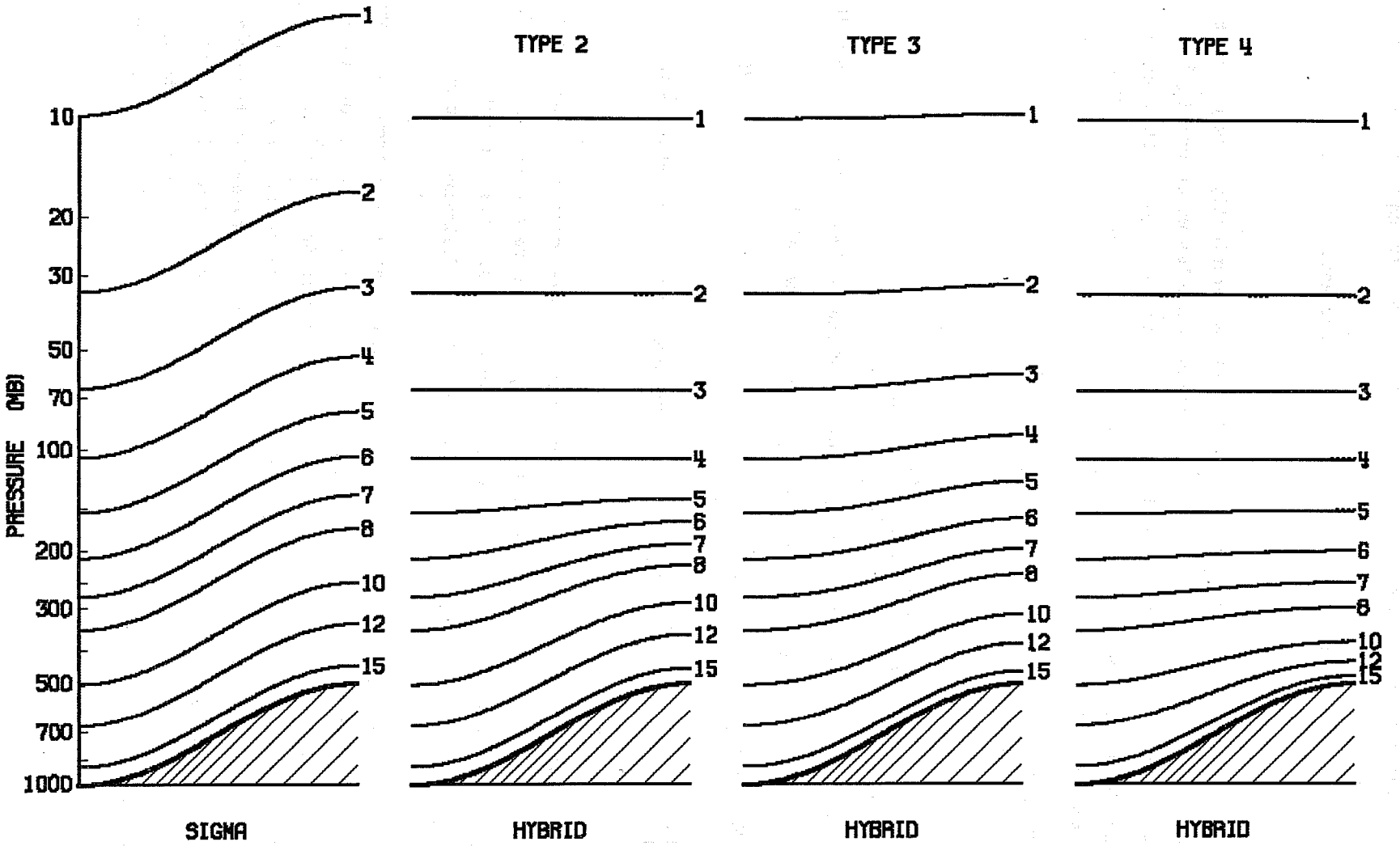

Fig. 1 Representation of the pressure variation along co-ordinate surfaces for sigma co-ordinates and alternative hybrid co-ordinates

The variation of coordinate levels for the four coordinates is compared in Figure 1 for selected levels of an 18-level resolution defined in the following section, and for a surface pressure varying from 1013.2 mb to 500 mb. The distribution of levels is chosen to be identical for the pressure of 1013.2 mb. For coordinate type 2 the interfacial pressure $P_{I+\frac{1}{2}}$ is given by I=4, and for this coordinate, Figure 1 illustrates how layer thicknesses vary sharply across the interface for values of the surface pressure typical of those occuring over high terrain. Coordinate 3 gives more smoothly varying layer thicknesses and small variations in pressure on the uppermost coordinate surfaces. The top 3 levels are pressure levels for coordinate 4, and layer thicknesses vary smoothly below these levels giving generally flatter coordinate surfaces and a fine low-level resolution over high ground. Values of the $A_{k+\frac{1}{2}}$ and $B_{k+\frac{1}{2}}$ in (5.1) may evidently be adjusted to give still flatter upper-level resolution over high ground, and in practice a balance must be found between the desirability of having coordinate surfaces as close as possible to pressure surfaces,and the possible disavantages in computational stability and accuracy associated with the fine, and rapidly-varying, low level resolution over mountains.

6. VERTICAL RESOLUTIONS

In subsequent sections we present a sample of results of idealized tests of the different coordinates and finite-difference schemes. For illustrative purposes attention is concentrated on one particular distribution of unequally-spaced vertical levels, although comparisons have been made with lower and higher resolution results obtained using an equal layer spacing.

The unequal distribution of levels is that used for operational forecasting with a sigma-coordinate model at ECMWF. 15 full levels are used and half-level values of η are given by

$$\eta_{k+\frac{1}{2}} = .75S_k + 1.75S_k^3 - 1.5S_k^4 , \quad S_k = k/NLEV. \tag{6.1}$$

Values of $P_{I+\frac{1}{2}}$ for hybrid coordinate 2 are chosen such that half-level pressures are identical to those of the sigma-coordinate and of the hybrid coordinate 3 for a surface pressure of 1013.2mb. Computations are performed for the interface at $\eta_{2\frac{1}{2}}$ and $\eta_{4\frac{1}{2}}$, that is at pressures of 105 and 229mb respectively. Thus layer thicknesses vary smoothly for the surface pressure of 1013.2mb, but exhibit an abrupt variation for surface pressures representative of those occuring over high ground. The $A_{k+\frac{1}{2}}$ and $B_{k+\frac{1}{2}}$ for coordinate 4 are defined by polynomials in S_k of degree 5 determined by requiring that half-level pressures coincide with those of the other coordinates for a surface pressure of 1013.2mb, that the top two interior levels ($1\frac{1}{2}$ and $2\frac{1}{2}$) are levels of constant pressure, and that the lowest two layers have half the thickness for a surface pressure of 500mb

that they have for the surface pressure of 1013.2mb.

Half-level values of pressure are given in Table 1 for surface pressures of 500 and 1013.2mb. The features evident in Figure 1 may also be seen in this Table. The sharp change in layer thickness across the interface which occurs with the traditional hybrid coordinate is particularly evident for coordinate 2b, and becomes more marked as the interface is lowered further.

	Coordinate Type, Ps 500 mb					All coordinates P_s = 1013.2mb
k	1	2a	2b	3	4	
1	25	51	51	47	51	51
2	52	105	105	89	105	105
3	81	131	164	129	159	164
4	113	159	229	169	210	229
5	148	190	253	210	257	300
6	187	224	280	250	301	379
7	228	261	310	290	339	463
8	272	299	340	329	373	551
9	317	339	372	366	403	642
10	361	378	403	401	429	732
11	403	415	432	433	452	817
12	441	448	458	460	471	893
13	471	475	480	481	486	955
14	492	493	495	495	496	998
15	500	500	500	500	500	1013

Table 1. Half-level values of pressure, $P_{k+\frac{1}{2}}$, in mb. Coordinate type 1 is the sigma-coordinate, 2a refers to the interfacial pressure of 105 mb and 2b to the interfacial pressure of 229 mb. Types 3 and 4 are the continuous hybrid coordinates specified in the text.

Alternative values for full level pressures are given in Table 2 for the 1013.2mb surface pressure. (a) and (b) refer to results calculated according to (3.17) and (3.18) (with C=1), (c) gives the arithmetic means of full-level values, while (d) gives results calculated from full-level values η_k computed from the same formula as (6.1) but with $S_k = (k-\frac{1}{2})/NLEV$.

The alternative full-level pressures are evidently very similar away from the upper and lower boundaries, the values (b) lying between those of (a), (c) and (d), while top-level differences are as anticipated in section 3 g). The rapid variation in layer thicknesses at low levels, chosen for the parameterization of boundary layer processes, results in the difference between the bottom full-level pressure and the surface pressure being a factor of two different when calculated from (6.1) as compared with the value implied by the finite-difference scheme. Since (6.1) is used in the operational version of the ECMWF model, it thus appears that, in this model, there is a difference of a factor of 2 in the height of the lowest full model level between that used in the boundary layer parameterization and that implied by the finite-difference scheme.

	P_k (mb)			
k	(a)	(b)	(c)	(d)
1	26	19	26	25
2	75	77	78	78
3	132	133	134	134
4	194	195	196	195
5	263	264	264	264
6	338	339	339	339
7	419	420	421	420
8	506	506	507	507
9	595	596	597	597
10	686	686	687	687
11	774	774	774	775
12	855	855	855	857
13	924	924	924	926
14	976	976	976	979
15	1005	1005	1005	1009

Table 2. Alternative full-level values of pressure for a surface pressure of 1013 mb.

In the following sections we adopt expression (3.18) with $C = 1$ at all but the top level, where we take $P_1 = \frac{1}{2}\Delta p$. Tests for the idealized calculations indicate that results are generally insensitive to this choice. It was decided, however, to use modified resolutions for experiments with the full forecast model. These were such that the thickness of the lowest layer was halved, thus giving a height of the lowest full-level similar to that assumed in the operational use of the boundary layer parameterization.

16 and 18 resolutions were used for the forecast experiments. Half-levels were determined by alternative polynomials of degree 4 in S_k, and full level pressures are compared with those of the 15 level resolution in Table 3. The 16-level resolution is generally finer below 500mb, particularly near the surface for reasons discussed above. The 18-level resolution is chosen to be very close to the 16-level resolution at troposheric levels, but extends higher into the stratosphere, with a top level at 10mb. This resolution is used only for hybrid coordinates since analysed data are unavailable above 10mb.

For the 16-level resolution coordinate 4 was constructed as described above for the 15-level resolution, while for the 18-level resolution polynomials of degree 6 were used with the top 3 levels being levels of constant pressure.

	NLEV	
15	16	18
		10
		33
25	25	65
77	77	105
133	136	154
195	200	211
264	270	276
339	345	348
420	423	425
506	506	506
596	590	590
686	673	673
774	754	754
855	830	830
924	896	896
976	951	951
1005	990	990
	1009	1009

Table 3. Full-level pressures in mb for 15, 16 and 18 level resolutions for a surface pressure of 1013.2 mb.

7. CANCELLATION OF GEOPOTENTIAL AND PRESSURE GRADIENT TERMS OVER STEEP OROGRAPHY

Reference has been made in the introduction to a number of authors who have examined the error in the representation of the pressure gradient over steep orography, and we repeat such calculations here in order to compare the hybrid and sigma-coordinates.

We consider a temperature field which is a function of pressure alone. In the continuous formulation the last two terms on the left hand-side of (2.1) cancel exactly. Noting that

$$\nabla\phi_s = \frac{RT(p_s)}{p_s}\ \nabla p_s$$

the corresponding finite-difference value of the sum of the two terms may be written:

$$\begin{aligned} E_k(p_s)\nabla p_s = &- \frac{RT(p_s)}{p_s}\ \nabla p_s + \alpha_k\, R\nabla T_k + RT_k \left(\frac{\partial \alpha_k}{\partial p_s}\right) \nabla p_s \\ &+ \sum_{j=k+1}^{NLEV} R\{(\nabla T_j)\ \ell n \frac{p_{j+\frac{1}{2}}}{p_{j-\frac{1}{2}}} + T_j \left[\frac{1}{p_{j+\frac{1}{2}}} \left(\frac{\partial p}{\partial p_s}\right)_{j+\frac{1}{2}} - \frac{1}{p_{j-\frac{1}{2}}} \left(\frac{\partial p}{\partial p_s}\right)_{j-\frac{1}{2}}\right]\nabla p_s \} \\ &+ \frac{RT_k}{\Delta p_k} \{(\ell n \frac{p_{k+\frac{1}{2}}}{p_{k-\frac{1}{2}}}) \left(\frac{\partial p}{\partial p_s}\right)_{k-\frac{1}{2}} + \alpha_k \left[\left(\frac{\partial p}{\partial p_s}\right)_{k+\frac{1}{2}} - \left(\frac{\partial p}{\partial p_s}\right)_{k-\frac{1}{2}}\right] \} \nabla p_s\ , \end{aligned} \tag{7.1}$$

where

$$\nabla T_k = \left(\frac{dT}{dp}\right)_{p=p_k} \left(\frac{\partial p_k}{\partial p_s}\right) \nabla p_s\ .$$

In evaluating these expressions we calculate $\partial\alpha_k / \partial p_s$ and $\partial p_k / \partial p_s$ from values of $(\partial p / \partial p_s)_{k-\frac{1}{2}}$ and $(\partial p / \partial p_s)_{k+\frac{1}{2}}$ using (3.9) and (3.17) or (3.18).

The error function $E_k(p_s)$ has been calculated for a number of temperature profiles, and we concentrate on results for the profile shown in the left-hand plot of Figure 2. This profile comprises three segments in which the temperature depends linearly on ℓnp. The relatively sharp tropopause results in the possibility of significant stratospheric error, for reasons discussed by Sundqvist (1976).

Plots of error are represented in figure 3 for the 15-level resolution specified in the preceding section with p_s = 750mb. For display purposes, this error is expressed dimensionally as a geostrophic wind error assuming $f = 10^{-4}s^{-1}$ and a large, though not unrealistic surface pressure change of 10% over 100 km .

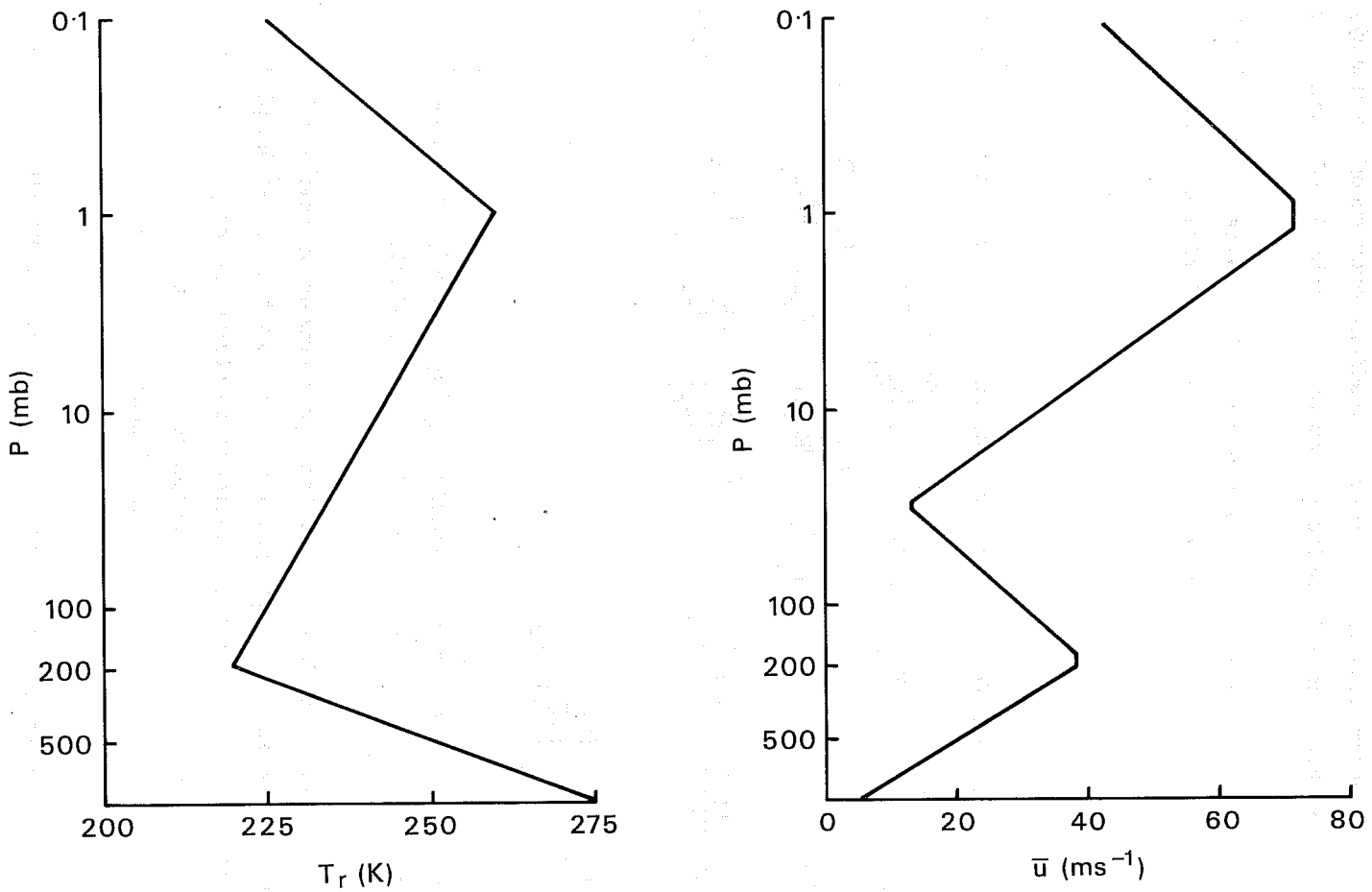

Fig. 2 A reference temperature profile, and the balanced zonal-mean flow used in quasi-geostrophic calculations

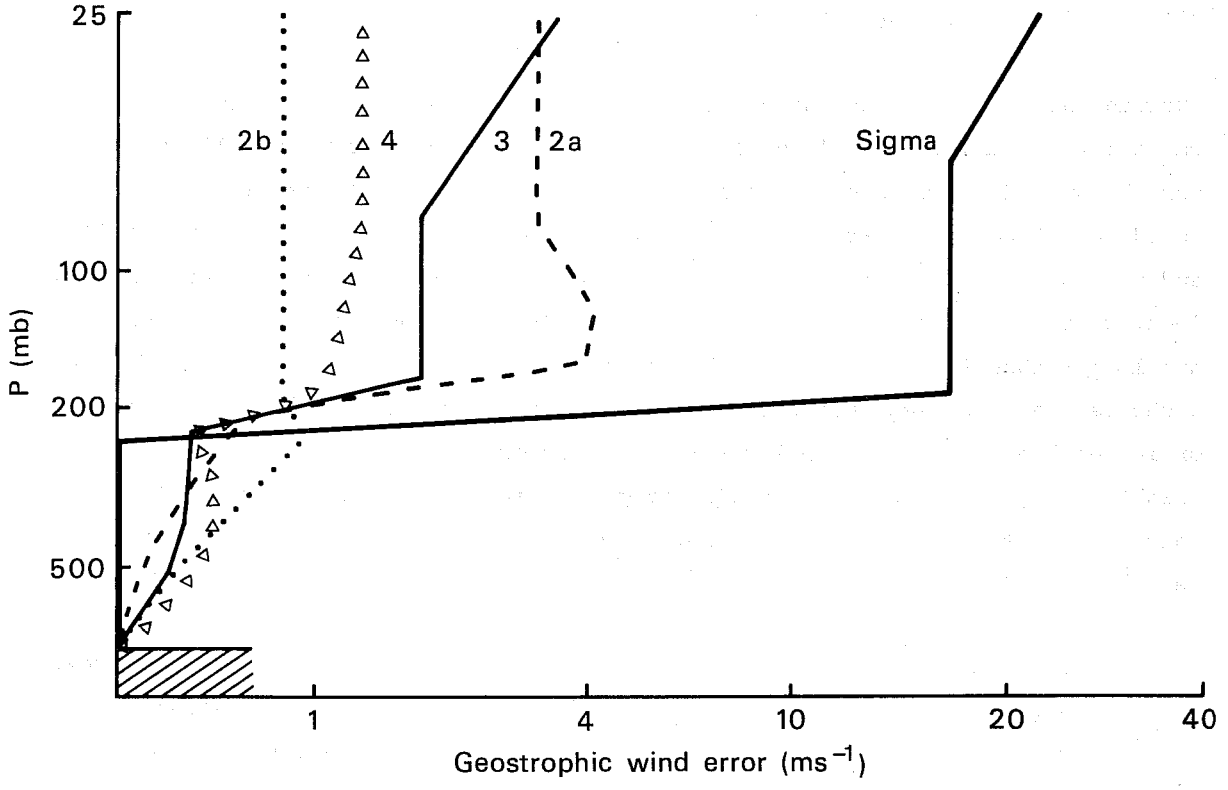

Fig. 3 The variation with height of the geostrophic wind error associated with error in the representation of the geopotential and pressure gradients. Curves are labelled by coordinate type as specified in Table 1.

In all cases the tropospheric error is low for this vertical finite-difference scheme. In particular it vanishes identically for the sigma-coordinate case. It is a matter of simple algebra to demonstrate that choosing definition (3.18), with C = 1, the pressure gradient error vanishes identically for a temperature profile $A\ell np + B$. A similar result for a different finite-difference scheme has been presented by Corby et al. (1972). It should be noted, however, that this result assumes the temperature profile to be known. If it is deduced from the geopotential using the finite-difference form of the hydrostatic equation, an error will result in this case also (Mesinger, 1981).

Substantial variations in the error above the tropopause are shown in Figure 3. The error is particularly large for the sigma-coordinate, and generally smaller for the hybrid coordinates. A consequence of the form of the traditional hybrid coordinate type 2 is that the error is independent of height above the interface, and we thus find particularly small stratospheric errors when the interface is located at the tropospheric pressure $p_{I+\frac{1}{2}} = 229mb$, although errors below this level are larger than found for the other coordinates. Some other disadvantages of such a choice are discussed in the following section. Comparisons of results for coordinates 3 and 4 show a smaller stratospheric error for coordinate 4, but a slightly larger (though still small) tropospheric error. Repetition of these calculations for the 18-level resolution discussed earlier gives very similar results.

For the sigma-coordinate case the stratospheric error is independent of pressure at all but the top level. This is again a consequence of the logarithmic temperature profile. The increase in the error at the topmost level is due to the choice $p_1 = \frac{1}{2} \Delta p$, rather than the form (3.18) with C = 1. It may, however, be removed by adopting the modification (3.19) to the calculation of the topmost geopotential.

The calculations shown in Figure 3 have been repeated for two approximations to the pressure gradient term which might be chosen as simpler alternatives to the angular momentum conserving scheme given by (3.10). In these calculations $(\nabla \ell np)_k$ is calculated either as $\nabla \ell n(\frac{1}{2}(p_{k+\frac{1}{2}} + p_{k-\frac{1}{2}}))$ or $\nabla\{\frac{1}{2}(\ell np_{k+\frac{1}{2}} + \ell np_{k-\frac{1}{2}})\}$. Resulting errors in the pressure gradient are compared with those for the angular-momentum conserving scheme in the upper plot of Figure 4, and show these alternative schemes to be generally associated with substantially larger errors.

Generally larger tropospheric errors are also found if the temperature profile includes an inversion (Mesinger, 1981). The calculation illustrated in Fig. 3 has been repreated for a temperature profile identical above 800mb, but with the sign of the vertical gradient reversed below 800mb. Results for a surface pressure of 900mb are shown in the lower plot of Figure 4, and these now indicate a clear

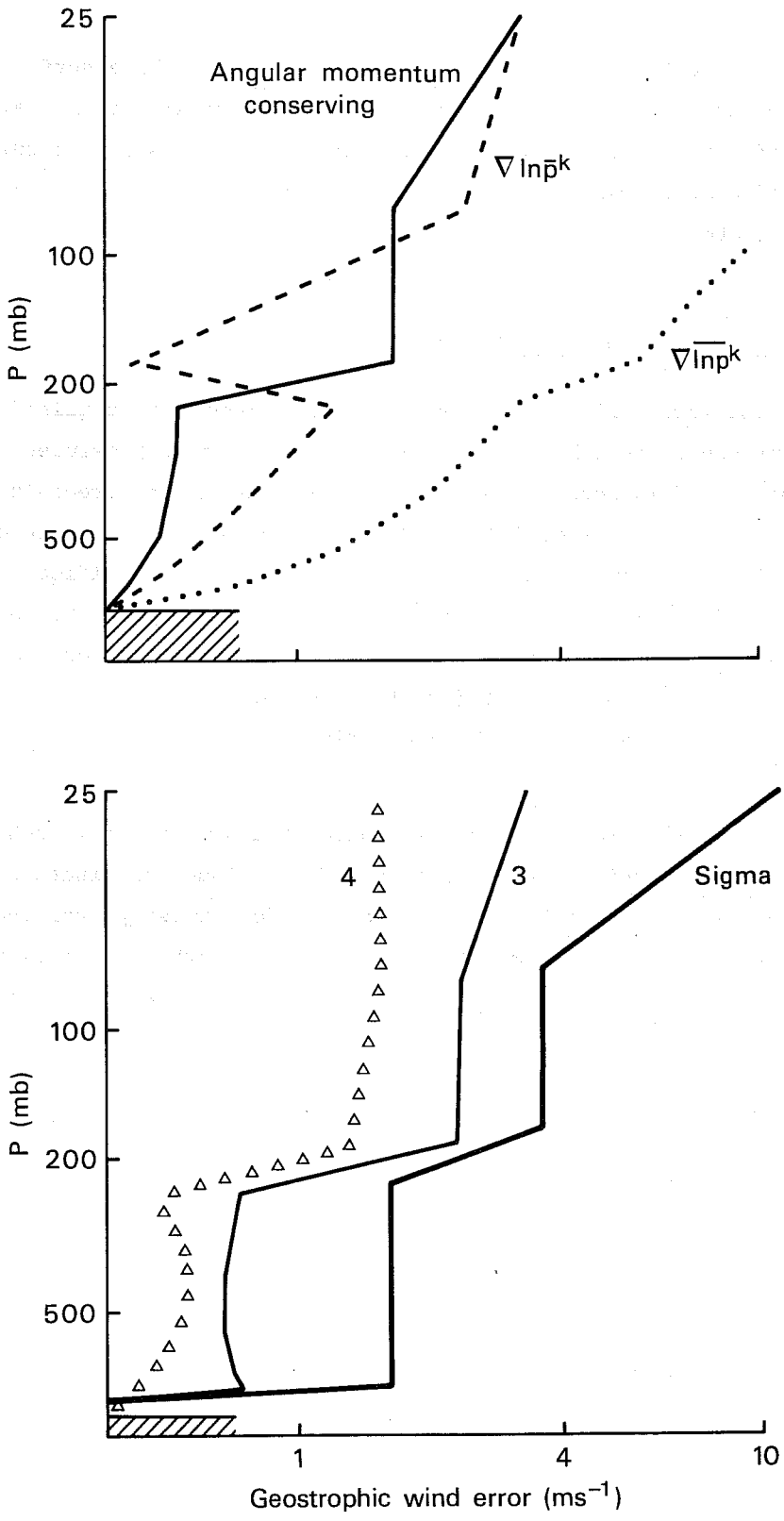

Fig. 4 As Figure 3, but for hybrid coordinate type 3 with alternative representations of the pressure gradient term (upper), and for sigma and continuous hybrid coordinates with a temperature profile with reversed gradient below 800 mb (lower).

advantage for the hybrid coordinates at troposheric levels. For a surface pressure of 1013.2mb, however, the tropospheric error is found to be similar for all coordinates, and of a magnitude about twice that shown for the sigma coordinate in the lower plot of Fig. 4. The stratospheric error remains substantially smaller for the hybrid coordinates.

8. STABILITY OF THE SEMI-IMPLICIT TIME SCHEME

Phase speeds of the lowest five gravity-wave modes, computed as outlined in section 4, are presented in Table 4 for two different surface pressures. The temperature profile and 15-level resolutions are as used in the preceding section. Phase speeds are found to be almost identical for the surface pressure of 1013.2mb, for which half-level pressures are identical, but significant differences are seen for the surface pressure of 500mb, larger differences between speeds for the two surface pressures being found for the hybrid coordinates. Following the results obtained by Simmons et al.(1978), this suggests that the semi-implicit time scheme may be less stable for hybrid coordinate systems.

We have thus examined the stability of the generalized semi-implicit scheme described in section 4 precisely as carried out for a sigma-coordinate scheme by Simmons et al. In each case stability was examined for timesteps varying from 5 to 60 minutes, in increments of 5 minutes, assuming a length scale equivalent to the smallest retained scale in a spectral model with triangular truncation at wavenumber 63.

	Coordinate type				
p_s (mb)	1	2a	2b	3	4
	309	309	309	309	309
	183	183	183	183	183
1013.2	82	82	82	82	82
	48	48	48	48	48
	30	30	30	30	30
	303	302	301	302	302
	185	166	166	169	166
500	94	71	71	75	71
	51	36	34	38	35
	32	24	21	25	22

Table 4. Phase speeds of the lowest five gravity-wave modes for two values of the surface pressure. Coordinate types are as in Table 1.

Results are summarized in Table 5 for the temperature profile shown in Figure 2. The hybrid coordinates in which the layer thicknesses vary continuously (types 3 and 4) appear to be little more prone to instability than the sigma-coordinate, but the possibility of instability becomes more marked for the traditional hybrid coordinate (type 2), particularly when the interface is located in the troposphere.

		Coordinate type				
P_s (mb)	P_r (mb)	1	2a	2b	3	4
1013.2	1013.2	S	S	S	S	S
750	1013.2	S	S	S	S	S
500	1013.2	S	S	35	S	S
1013.2	750	S	45	50	S	S
750	750	S	S	S	S	S
500	750	S	S	45	S	S
1013.2	500	5	5	5	5	5
750	500	S	25	5	60	5
500	500	S	S	S	S	S

Table 5. The stability of the semi-implicit scheme. S denotes stability for all timesteps examined, while unstable cases are denoted by the smallest timestep for which instability is found. Coordinate types are as in Table 1. An isothermal reference temperature of 300K is used (as elsewhere in this report).

It should be noted that the semi-implicit scheme outlined in section 4 is formulated using as a variable the deviation of surface pressure from its reference value. Most of the practical tests of the hybrid coordinates have utilized the ECMWF grid-point model for which the standard semi-implicit scheme works with the logarithm of the surface pressure. In this case the vectors $\underset{\sim}{h}_1$ and $\underset{\sim}{h}_2$ should be multiplied by the reference surface pressure p_r, and $\underset{\sim}{\nu}$ should be divided by p_r. Non-linear terms change accordingly.

Use of this logarithmic form results in no change to gravity-wave phase speeds as (4.5) shows the vectors $\underset{\sim}{\nu}$, $\underset{\sim}{h}_1$ and $\underset{\sim}{h}_2$ to appear in the form of the product $(h_1+h_2).\underset{\sim}{\nu}$, but a pronounced change in the stability of the semi-implicit scheme results. Table 6 presents results in this case, and comparison with Table 5 shows that the hybrid schemes are much more prone to instability when the logarithmic form is used.

Ps	Pr	Coordinate Type				
(mb)	(mb)	1	2a	2b	3	4
1013.2	1013.2	S	S	S	S	S
750	1013.2	S	30	20	25	20
500	1013.2	S	15	10	15	10
1013.2	750	S	S	S	S	S
750	750	S	S	S	S	S
500	750	S	20	15	S	15
1013.2	500	S	45	5	25	5
750	500	S	S	S	S	S
500	500	S	S	S	S	S

Table 6. As Table 5, but for a formulation of the semi-implicit scheme in which the equations are linearized about $\ell n p_r$.

This instability may be understood by reference to the form of (4.3) for small amplitude gravity wave motion:

$$\frac{\partial p_s'}{\partial t} = (\underset{\sim}{\nu} - \underset{\sim e}{\nu}).\underset{\sim}{D} - \underset{\sim}{\nu}.\underset{\sim}{D}$$

where $(\underset{\sim}{\nu})_j = (\Delta p_j)_{p_s = p_r}$ and $(\underset{\sim e}{\nu})_j = (\Delta p_j)_{p_s = p_e}$,

where the latter term represents the layer thickness evaluated for the exact basic surface pressure, p_e, upon which the small amplitude motion is superposed. The corresponding logarithmic form is

$$\frac{\partial \ell n p_s'}{\partial t} = (\frac{\underset{\sim}{\nu}}{p_r} - \frac{\underset{\sim e}{\nu}}{p_e}).\underset{\sim}{D} - \frac{\underset{\sim}{\nu}}{p_r}.\underset{\sim}{D}$$

It is likely that the greater instability in the latter case arises because at upper levels, where the instability characteristically develops (Simmons et al., 1978), the hybrid coordinate surfaces are surfaces of constant pressure and thus $(\underset{\sim}{\nu}) \simeq (\underset{\sim e}{\nu})$.

The instability indicated by the above analysis has been realized in practice. Initial tests of the difference schemes given in sections 2 and 3 were performed using an adiabatic version of the grid-point model described by Burridge and Haseler (1977) together with the partially implicit fourth-order horizontal diffusion scheme used in operational forecasting since March, 1980. Integrations were performed from an analysis for 16 January, 1979 using the 15-level vertical resolution and a horizontal resolution of 3.75° (N24) for the regular latitude-longitude grid.

Using the logarithmic version of the semi-implicit scheme and a reference surface pressure of 1013.2mb, stable 10-day integrations were performed for the sigma coordinate and the continuous hybrid coordinate, type 3. However, an integration for the traditional hybrid coordinate with an interface at 229mb (type 2b) became unstable after about 3½ days. Stable 10-day integrations were completed in this case by using the logarithmic version with an 800mb reference pressure, and also by using the theoretically more stable scheme given in section 4 with a reference pressure of 1013.2mb. Further examples will be discussed later in the context of experiments using the complete forecast model.

Examining the stability of the semi-implicit scheme for a tropospheric lapse rate larger than shown in Figure 2 reveals a further possible problem for the hybrid coordinate type 2. In this case an unstable gravity-wave mode was found for a surface pressure of 500mb when the interface was located in the troposphère, whereas all modes were stable for a stratospheric interface, and also when calculated using the sigma and alternative hybrid coordinates. This may be readily understood by examining the form (3.4) chosen for the vertical advection terms to ensure conversation. If the "vertical velocity", $\dot{\eta}\partial p/\partial \eta$, varies slowly with pressure the finite-difference approximation to $\partial T/\partial p$ at level k is

$$\frac{1}{2\Delta p_k}\,(T_{k+1} - T_{k-1})$$

If Γ is the actual gradient at level k this finite-difference form may be written approximately as

$$\frac{p_{k+1} - p_{k-1}}{2\,\Delta p_k}\,\Gamma \approx \{\tfrac{1}{2} + \tfrac{1}{4}\,(\,\frac{\Delta p_{k-1} + \Delta p_{k+1}}{\Delta\, p_k}\,)\}\,\Gamma$$

This evidently yields a good approximation to Γ if the layer thicknesses vary smoothly, but over the highest mountains thicknesses may vary by a factor of more than two across the interface. The temperature gradient may thus be overestimated by at least 25% immediately below the interface, and this can lead to gravitational instability if the interface is located in the troposphere. Immediately above the interface the gradient is underestimated by a similar amount.

9. REPRESENTATION OF FORCED PLANETARY-WAVE MOTION

Studies of the representation of forced long-wave motion have been made using a linearized, β-plane quasi-geostrophic model which uses the vertical coordinates and finite-difference scheme introduced in preceding sections. The quasi-geostrophic formulation is similar to that described by Simmons and Hoskins (1976) for a model with spherical geometry, the principal difference being that here we include additional terms involving surface-pressure gradients. The resulting continuous equations are equivalent to the modified quasi-geostrophic set with geometric height as vertical coordinate proposed by White (1977). Details of the finite-difference model are given in Appendix C.

Steady forced solutions for zonal wavenumbers 1 and 2 have been computed for the basic state representative of mid-latitudes shown in Figure 2. The forcing is loosely based on values chosen by Bates (1977), although heating rates are somewhat larger in magnitude. Specifically, the height of the orography is taken to be $350\cos(\lambda - 87°)$m for wavenumber 1 and $430\cos(2\lambda + 197°)$m for wavenumber 2, where λ is longitude. The diabatic rates of change of temperature are taken to be $10^{-5}\,(p/1000\text{mb})^2\cos(\lambda + 127°)$ and $2\times10^{-5}\,(p/1000\text{mb})^2\cos(2\lambda + 63°)$ Ks^{-1}

respectively. It should be noted that in view of the simplicity of the model used, and in particular its absence of any representation of latitudinal propagation, the absolute quantitative significance of results is doubtful. Rather, attention should be concentrated on the differences between results using different vertical coordinates.

Amplitudes are presented in Figure 5 for the sigma coordinate and hybrid coordinate type 3. The 15 level resolution is used as in earlier examples. Also shown is a high resolution reference calculation in which the uppermost levels are located in a region of mesospheric easterly winds, and which thus is insensitive to the misrepresentation of the upper boundary condition that occurs in models such as those considered here (see, for example Lindzen et al. 1968; Nakamura, 1976; Kirkwood and Derome, 1977; Bates, 1977).

Figure 5 reveals a qualitatively similar tropospheric structure for the three calculations, but some quite large quantitative differences. The error in the 15-level calculations is evidently sensitive to coordinate type, although this one calculation is not sufficient to demonstrate a general superiority of the hybrid coordinate. Comparison of phases shows smaller differences.

One interesting result of these forced-wave calculations is that differences between results for the various hybrid coordinates are much smaller than the differences between sigma and hybrid coordinate results shown in Figure 5. This is demonstrated by Table 7. It is likely that this reflects the fact that the principal error in the forced-wave structures is due to inadequate stratospheric resolution. The various hybrid coordinates are similar in the stratosphere, being exactly or almost exactly pressure, and this apparently results in a very similar error in the tropospheric structure of forced long waves.

Zonal Wavenumber	Coordinate Type	p(mb) 1005	506	195
1	1	.327(-119°)	.253(83°)	.634(85°)
1	2a	.344(-118°)	.209(81°)	.622(84°)
1	2b	.345(-119°)	.207(81°)	.644(84°)
1	3	.345(-119°)	.210(81°)	.638(83°)
1	4	.345(-119°)	.207(81°)	.639(83°)
2	1	.314(168°)	.458(10°)	.947(10°)
2	2a	.341(169°)	.378(9°)	.901(9°)
2	2b	.340(169°)	.379(9°)	.930(9°)
2	3	.339(168°)	.384(9°)	.924(9°)
2	4	.340(169°)	.380(9°)	.924(9°)

Table 7. The amplitude (in units of $10^7 m^2 s^{-1}$) and phase (bracketed) of the forced perturbation stream function at three pressure levels for two wavenumbers and the coordinate types specified in Table 1.

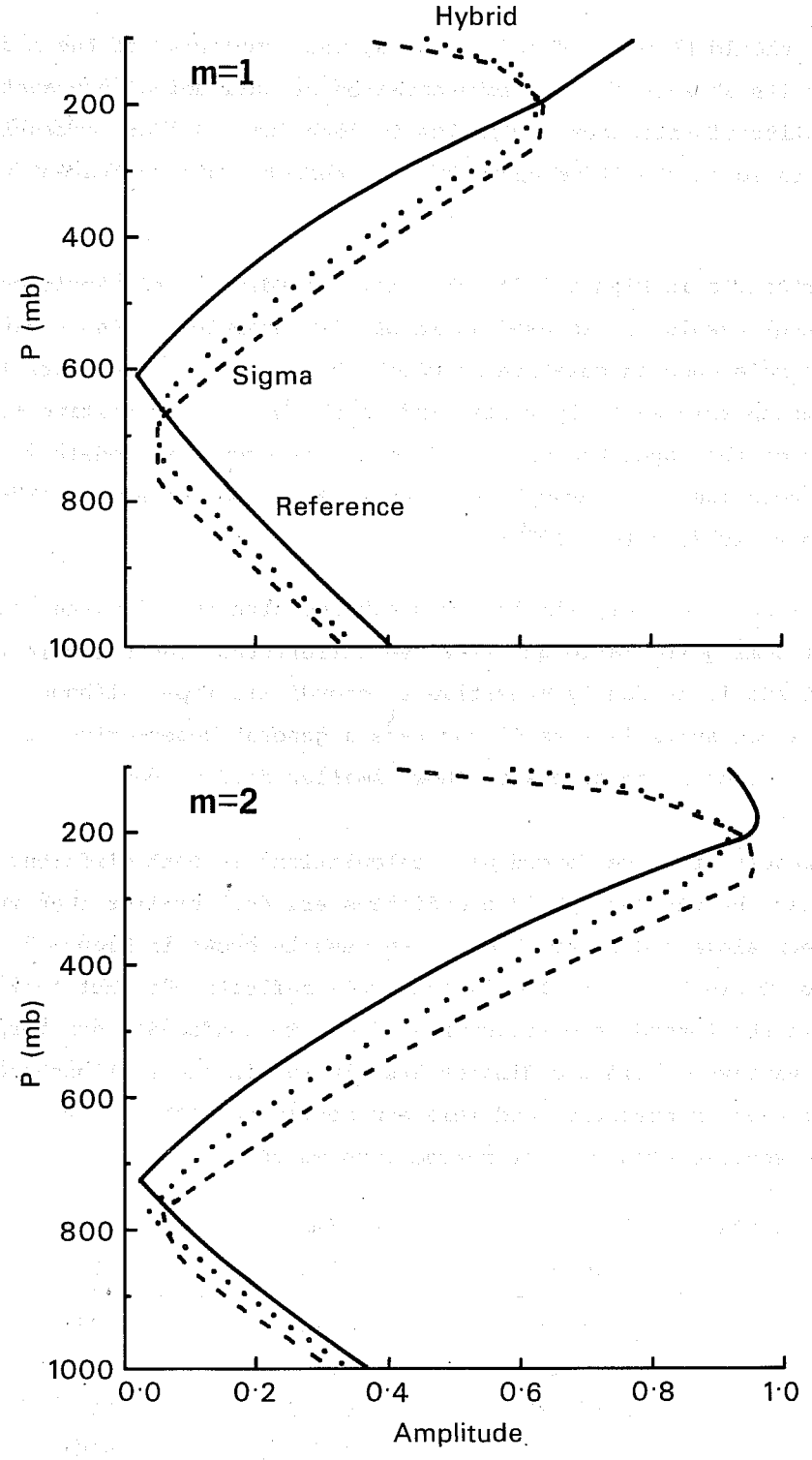

Fig. 5 The amplitude (in units of $10^7 m^2 s^{-1}$) of the perturbation stream function for zonal wavenumber 1 and 2 and the mean state shown in Figure 2. The solid curve is a reference 100-level sigma coordinate calculation with $\sigma_{k+\frac{1}{2}} = (k/100)^3$, the dotted curve is obtained for 15 levels using hybrid coordinate type 3 while the dashed curve shows the result for 15-levels using the sigma coordinate. A representative height-dependent Newtonian cooling was included in these calculations.

10. IMPLEMENTATION IN THE ECMWF GRID-POINT FORECAST MODEL

The general vertical finite-difference scheme has been included in the ECMWF grid-point forecast model. The modified form (3.19) for the calculation of the geopotential at the top model level was used, as was the full-level definition (3.18). The sigma coordinate scheme described by Burridge and Haseler (1977) was generalized in a natural way, a sigma coordinate term such as

$$\frac{1}{p_s a \cos\theta}\left(\overline{p_s}^{\lambda} u_k \; \delta_\lambda T_k\right)^{\lambda}$$

at level k becoming

$$\frac{1}{\Delta p_k \; a \cos\theta}\left(\overline{\Delta p_k}^{\lambda} \; u_k \; \delta_\lambda T_k\right)^{\lambda} .$$

Complete details will not be given here but we note that the general scheme reproduces Burridge and Haseler's horizontal scheme in the special case of sigma coordinates, and that the conservation properties of the horizontal scheme for general coordinates are similar to those for sigma coordinates.

The philosophy behind the implementation of the new scheme was to produce, for the purposes of initial research, as general a scheme as possible with a minimum of recoding of the operational model. Thus the physical parameterizations coded for sigma coordinates were implemented by defining, for each grid-point of the model, a local sigma coordinate with a resolution such that the sigma levels coincided with the general coordinate surfaces at the point in question. A result of this philosophy is that the general model carries a computational overhead of some 20 % when compared with the operational model. It must be stressed, however, that careful program design, restriction to a coordinate of form (5.1), and coding to omit terms which are zero for coordinate surfaces which are surfaces of constant pressure, should result in a substantially reduced overhead. Indeed, a hybrid model in which the majority of levels are levels of constant pressure, for example a model designed for predominantly stratospheric studies, should prove more efficient than a corresponding sigma coordinate model.

Initial data is constructed for the general vertical coordinate by interpolation of analyzed, pressure-level data to the model levels. Routines for full-field interpolation from pressure to sigma used operationally until December 1980 have been modified to achieve this. Normal-mode initialization routines have also been

modified to run with the general coordinate, using modes calculated as indicated in section 4. These routines, however, have not been used for most tests as initial gravity-wave amplitudes have been generally found to be little more than 1mb in surface pressure and to decay to negligible values over the first day or so of integration. It should be noted that the pressure-coordinate analyses where derived from data assimilation cycles using the standard sigma-coordinate model, and the experiments reported here thus do not test the complete impact that use of a hybrid coordinate might have when incorporated in the whole forecasting system.

Many of the routines used at ECMWF for the display, diagnosis and verification of forecast results use a post-processed form of forecast data which has been interpolated from sigma coordinates to standard pressure levels. Post-processing routines have accordingly been modified to transform data from the general coordinate surfaces to the standard pressure levels. Cubic spline fits using either σ or $\ell n\sigma$ (depending on the field to be interpolated) have been replaced by fits using η or $\ell n\eta$. In the case of coordinate 4, η is defined implicitly for a pressure ρ using the polynomial definitions of A and B:

$$\eta = A(s) + B(s)$$

where s satisfies

$$p = A(s)p_o + B(s)p_s.$$

A bisection method is used to compute s. Values of η so defined coincide with those for other coordinates when $p_s = p_o$. Comparisons of post-processed initial data for the various coordinates revealed negligible differences.

11. FORECAST CASES

Forecast experiments using a standard N48 horizontal resolution and a number of vertical coordinates and resolutions have been performed for four situations. Two (00GMT, 16 January 1979 and 00GMT, 17 February 1979) were chosen from analyses of FGGE data, and use the relatively smooth distribution of orography adopted for the initial phase of operational forecasting. The January case yields forecasts of above average quality, and has been extensively examined from a number of viewpoints (e.g. Bengtsson, 1981). The February case, conversely, gives below average results. Both situations are characterized by pronounced circulation changes in the stratosphere during the 10-day forecast period, and the simulation of these changes is examined in addition to the usual evaluation of the tropospheric forecasts.

The third and fourth cases use the rougher, more realistic distribution of orography introduced into operations at the beginning of April, 1981. The third (12GMT, 12 February 1981) was chosen from the final pre-operational benchmark of this orography, and gives forecasts of a quality similar to those from 16, January 1979. The fourth (12GMT, 5 April 1981) was chosen from the early phase of operational implementation. The operational forecast in this case was one of the poorest of the month.

It should be noted that in all cases sigma-coordinate data sets were reconstructed, and forecasts carried out, using the same procedures as adopted for the hybrid coordinates. This was done in order to minimize any bias towards the sigma coordinate in the forecast results.

12. FORECAST RESULTS

12.1 Objective verification

The anomaly correlation of the height field averaged over the extratropical troposphere of the northern hemisphere is shown in Figure 6 for the four chosen situtaions. In each case three forecasts are presented. The light solid lines refer to 16-level sigma-coordinate forecasts, the dashed lines to 16-level forecasts using hybrid coordinate type 4, and the dotted lines to corresponding 18-level hybrid coordinate forecasts in which the top full pressure level is raised from 25 to 10mb.

The results illustrated in Figure 6, and indeed many other objective measures, show that change from the sigma to the hybrid coordinate results in little overall change in forecast quality, although some differences are apparent in Figure 6. Anomaly correlations generally favour slightly the hybrid coordinate at days 4, 5 and 6. Beyond this time only two of the forecasts (16 January, 1979 and 12 February, 1981) are of a standard sufficiently high to judge forecast differences, and they give contrasting results. For 16 January the 18-level hybrid forecast appears distinctly more accurate than the 16-level hybrid forecast, which is itself slightly better than the sigma-coordinate forecast. Differences are somewhat smaller for 12 February but opposite in sign, the sigma-coordinate being favoured in this case. In both cases, however, the 16-level sigma- and hybrid-coordinate results are closer to each other than to the 18-level hybrid results near the end of the forecast period.

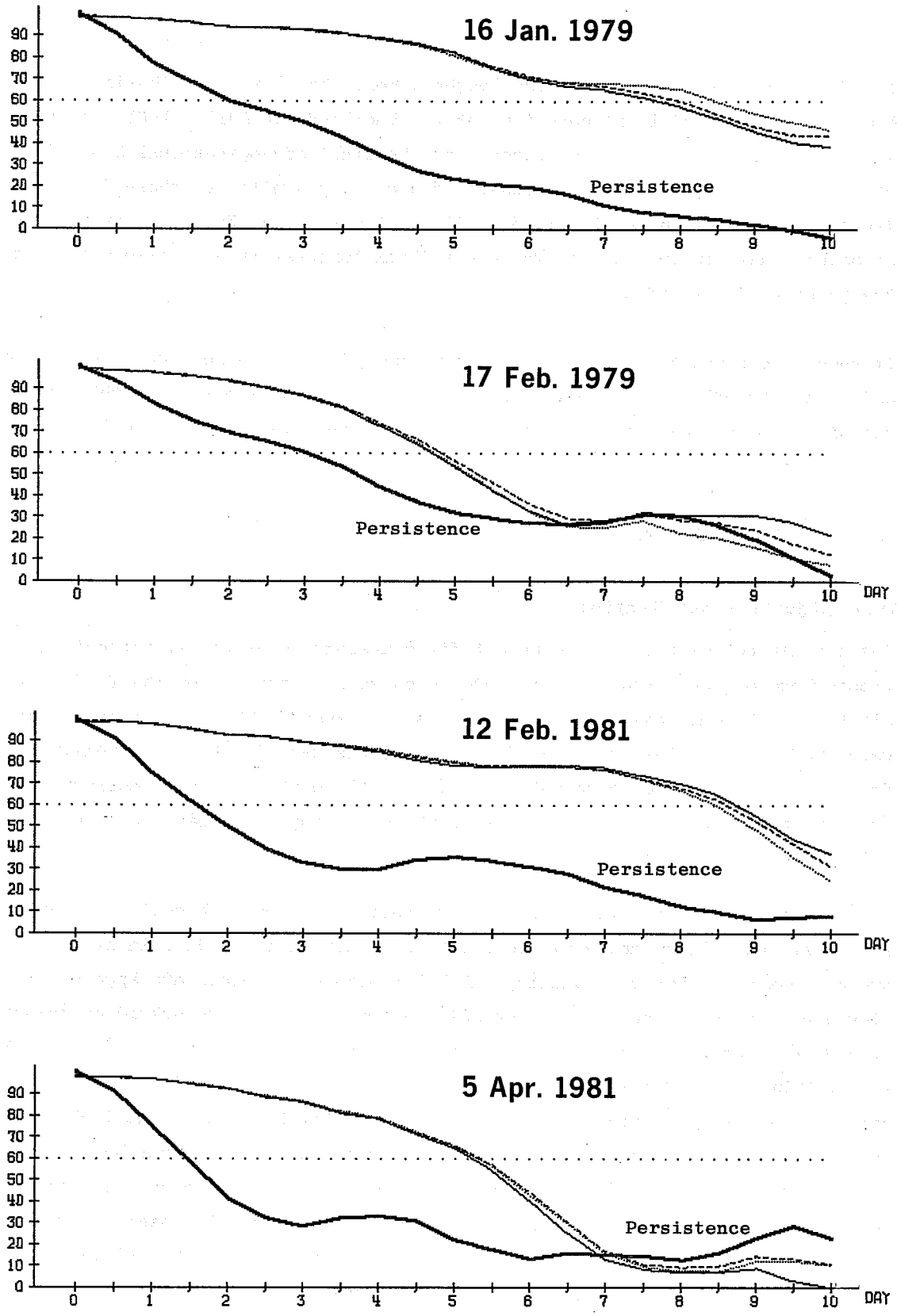

Fig. 6 Anomaly correlations of height (%) averaged from 1000 to 200 mb and from 20° to 82.5°N as functions of time. The initial date of each forecast situation is shown. The heavy solid curves show results from persistence forecasts, while the other curves represent the model forecasts specified in the text.

The performance of hybrid coordinate type 4 is compared with that of coordinate type 3, for which coordinate surfaces tend less rapidly to pressure surfaces as the pressure decreases, in Figure 7. Results are shown for both 16- and 18-level resolutions for the two FGGE cases. Forecasts are evidently extremely similar up to day 7, differences being much smaller than both differences between sigma- and hybrid-coordinate forecasts and differences between 16- and 18-level forecasts, as suggested by the linear, steady-state model. Marginally better results beyond day 7 are found for the flatter coordinate surfaces of type 4 in the 16 January case.

Some of the advantages of the hybrid coordinate over the sigma coordinate might be expected to be more marked at upper levels. Such an advantage is barely discernible in the objective verification of the height field, but may be seen clearly in the variation with height of the anomaly correlation of the temperature field. Figure 8 shows that while there may be variability in the relative performance of the two coordinates at lower levels, the hybrid coordinate consistently gives a lower error in the vicinity of the tropopause, a result found for both 16- and 18-level resolutions. A similar result has also been found in the comparison of grid-point and spectral forecasts (Girard and Jarraud, 1981), and may here be due to lower truncation error associated with the smaller variation of temperature along the pressure-like coordinate surfaces of the hybrid model close to the tropopause. Effects due to a more accurate pressure gradient and an effectively weaker "horizontal" diffusion(to be discussed later) may also contribute.

A systematic error of the operational ECMWF forecast model is its tendency to accelerate the subtropical jet stream in the lower stratosphere, as may be seen by inspection of Fig. 4.8 of monthly ECMWF Forecast Reports. Examination of this error for the four cases considered here shows it to be slightly larger for the hybrid coordinate than for the sigma coordinate, and larger for a 10mb top level than for a 25mb top level. This is illustrated for the 5 April case in Figure 9.

A second systematic error is the overall cooling of the model troposphere during the course of the forecast. This has been found to be similar in both sigma- and hybrid-coordinate forecasts. Extending the top-level to 10mb is, however, found to result in a significant increase in the zonal-mean temperature error at 50mb, although the error is reduced at 100 mb in the 5 April case shown in Figure 10. Reasons for the larger error at 50mb have not yet been thoroughly

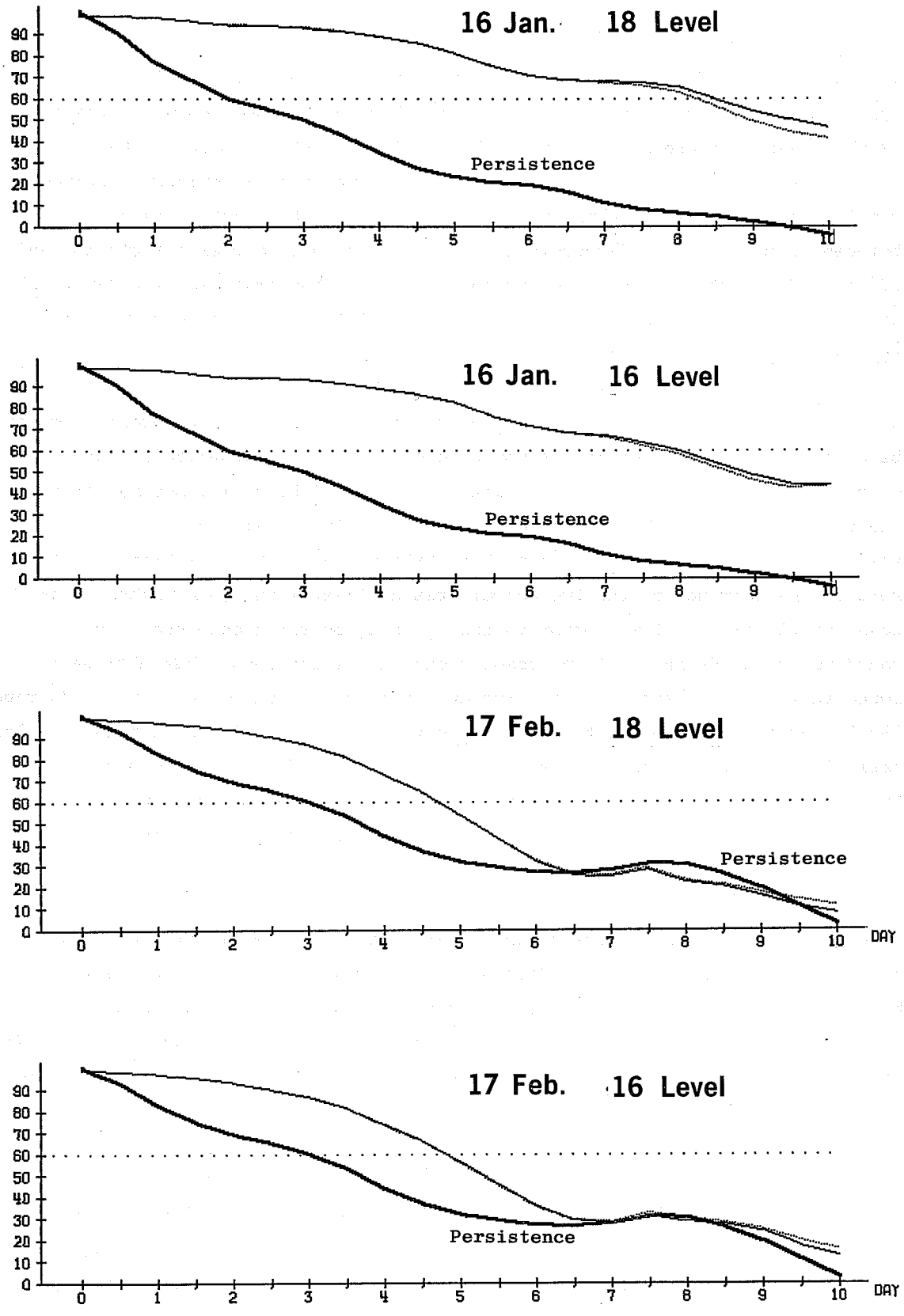

Fig. 7 Anomaly correlations of height (%) averaged from 1000 to 200 mb and from 20° to 82.5° N as functions of time. The light solid curves refer to results from hybrid coordinate type 4, and dotted curves to coordinate type 3.

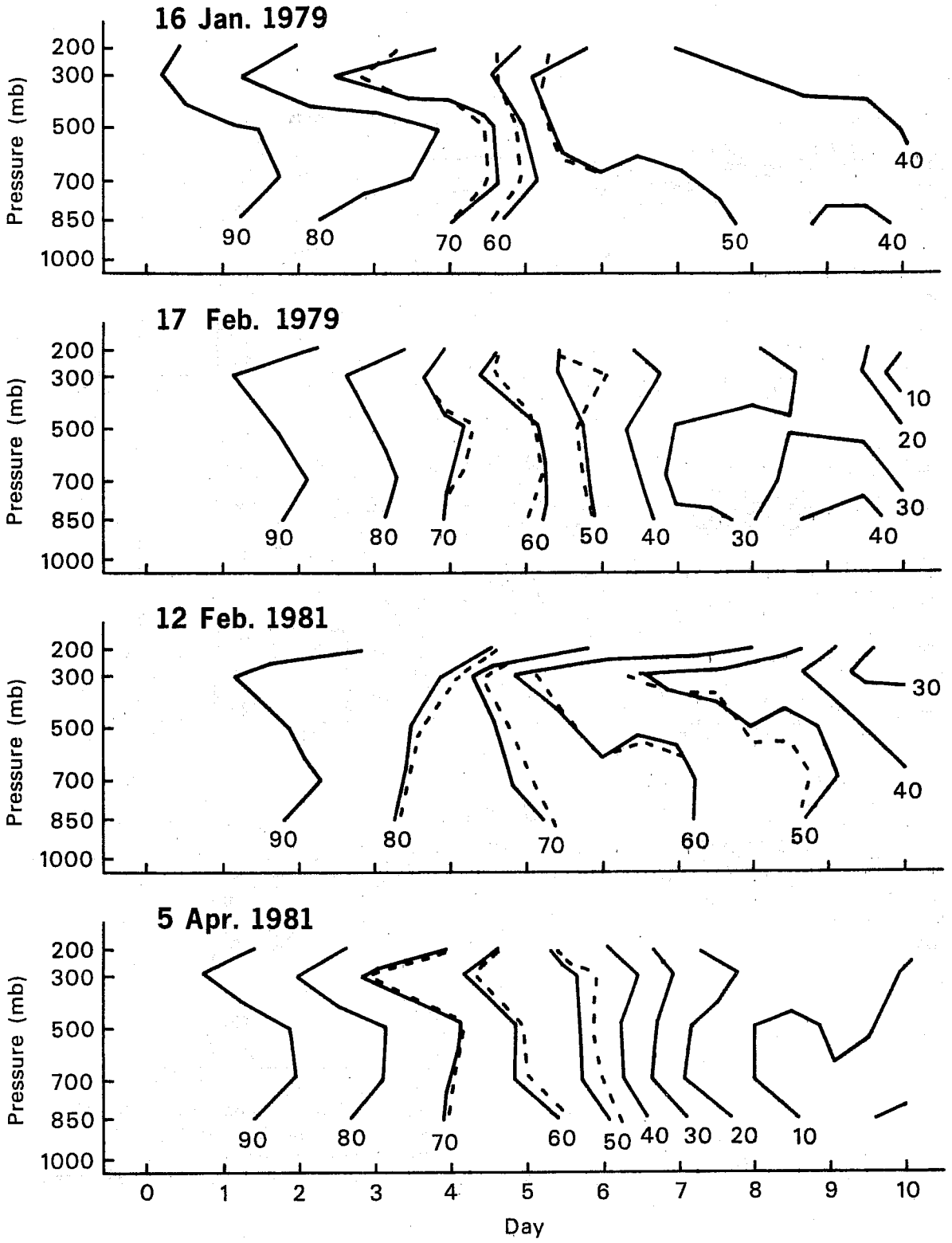

Fig. 8 Contour plots showing the dependence of anomaly correlation of temperature (%) averaged from 20°to 82.5°N on pressure and time. The solid curves refer to results for the sigma co-ordinate, while the dashed curves are obtained from 18-level forecasts using hybrid co-ordinate type 4.

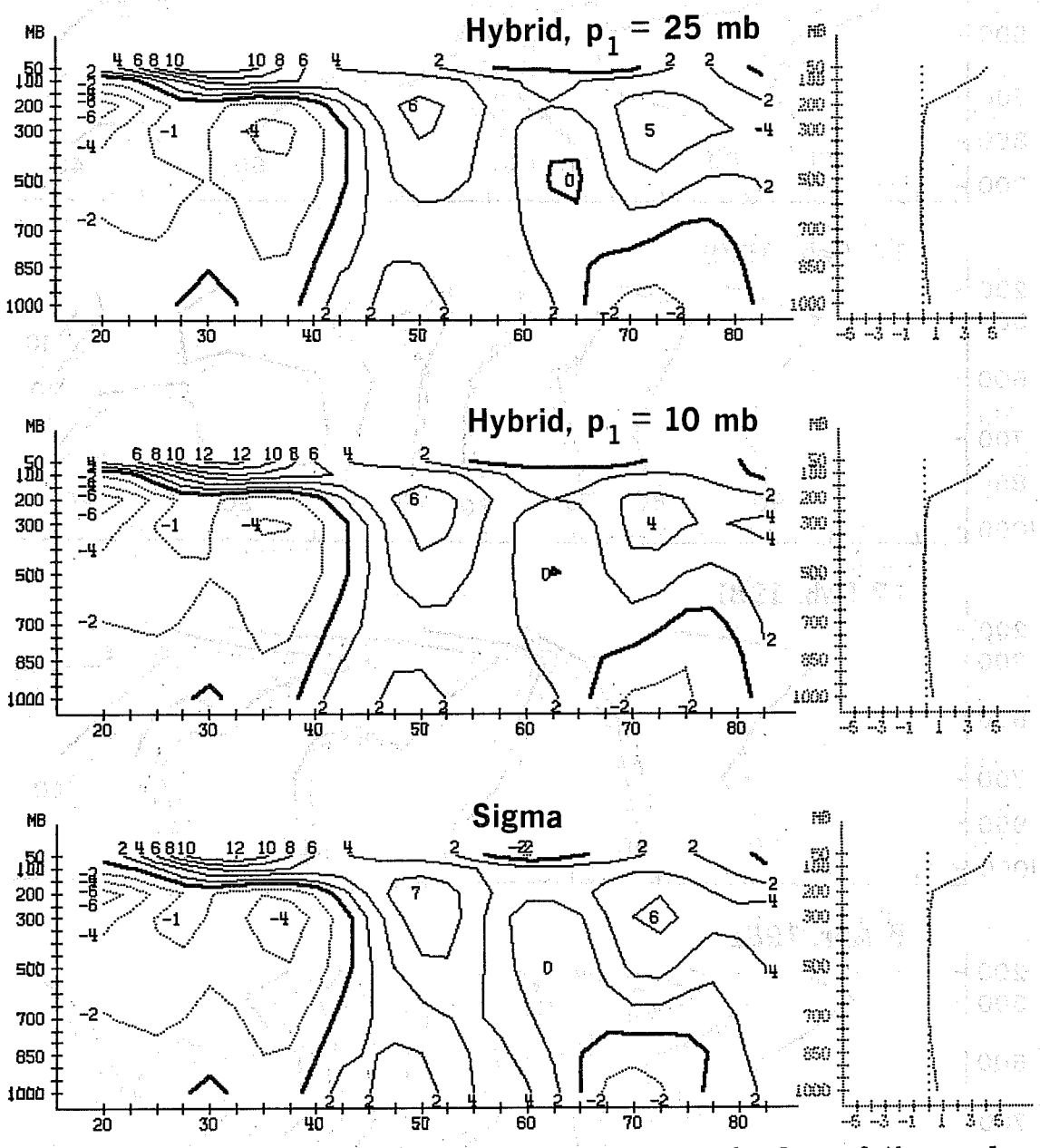

Fig. 9 The difference between forecast and observed values of the zonal-mean geostrophic wind (ms^{-1}) averaged over the last 5 days of the forecast from 12 February 1981. The hybrid forecasts used coordinate type 4. The right-hand plots show values averaged from 20^{o} to 82.5^{o} N.

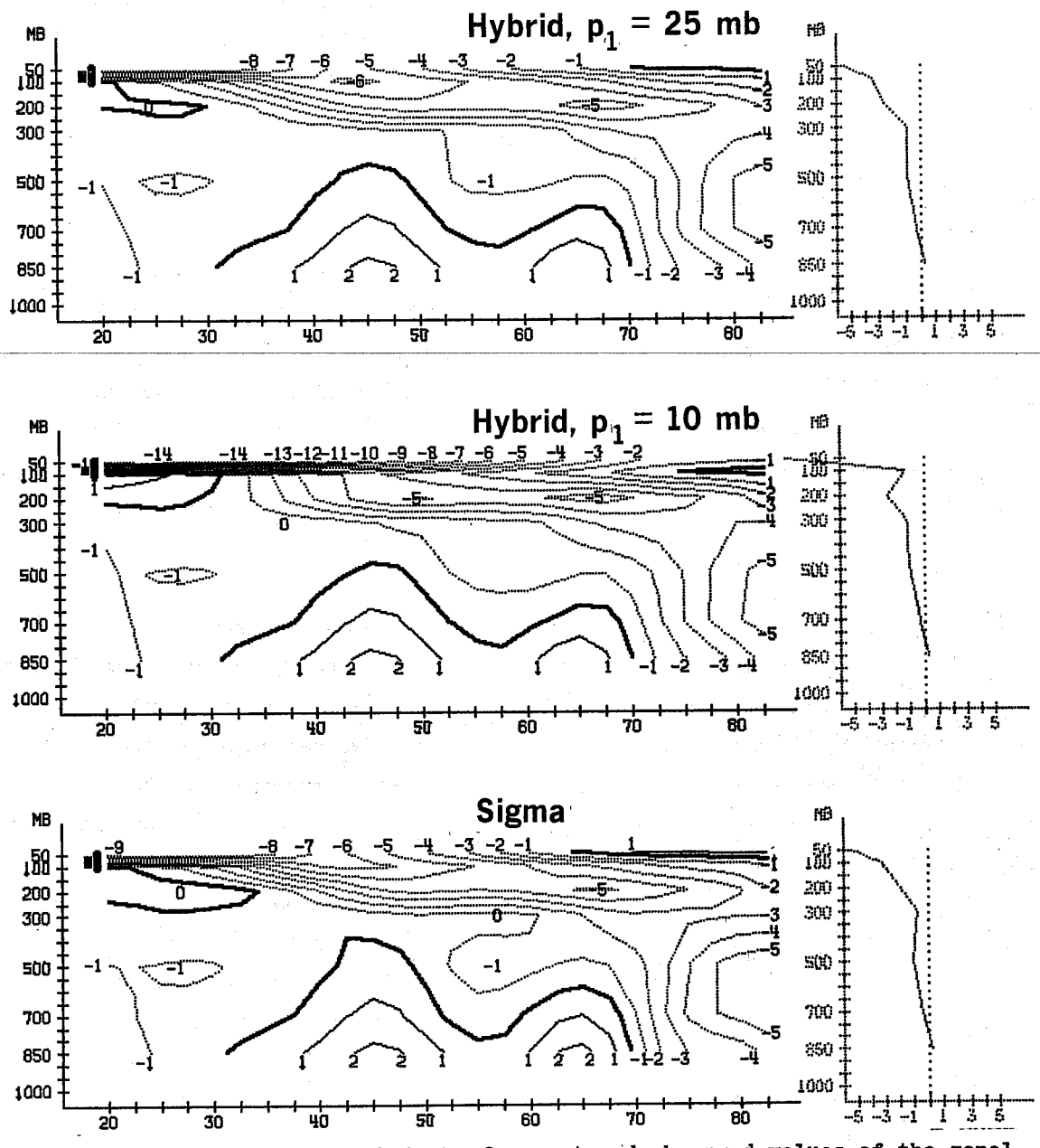

Fig. 10 The difference between forecast and observed values of the zonal-mean temperature (K) averaged over the last five days of the forecast from 5 April 1981. The hybrid forecasts used coordinate type 4.

investigated, but it appears not to be due to an inherent deficiency of the hybrid system. Rather, increasing the vertical resolution in the stratosphere gives rise to a spuriously large initial radiative cooling at the second model level from the top. Further study of this is taking place.

12.2 Synoptic assessment

The similarity in objective scores shown in Fig. 6 is seen also in a direct comparison of the forecast charts. The case which reveals the most sensitivity in this respect is 16 January, and maps of 1000mb height at day 6 and 500mb height at day 8 are presented in Figures 11 and 12. In these figures the operational FGGE analyses are compared with 16-level forecasts using the sigma coordinate and hybrid coordinate type 4, and with the corresponding 18-level hybrid forecast. The corresponding objective verification is that shown in the upper graph in Figure 6.

Both figures clearly show the various forecasts to be much closer to each other than any of them is to the analyzed state of the atmosphere, although some synoptic differences between the forecasts can be found. Comparing the 18-level hybrid forecast with the 16-level sigma-coordinate forecast we see at day 6 that the former has produced much less of a spurious double-low structure to the disturbance that has developed near the East Coast of North America, and has also produced three more distinctly separate high pressure centres over Europe and the North Atlantic. Its improvement over the sigma-coordinate forecast is more marked at day 8, it giving a better phase and orientation to the blocking high in the North Atlantic, to the ridge over the West Coast of North America, and to the three troughs downstream of this ridge. Differences elsewhere are much smaller. At both day 6 and day 8 the 16-level hybrid forecast can be seen to give results intermediate between those for the 18-level hybrid forecast and the sigma-coordinate forecast.

500mb height maps are shown in Figure 13 for day 8 forecasts from 12 February, 1981. Figure 6 indicates from an objective viewpoint a more accurate forecast for the sigma coordinate in this case, although differences at day 8 are smaller than for the 16 January. This is confirmed by Figure 13, which shows the sigma-coordinate forecast to give a better representation of the flow round the high pressure centre located over North Eastern Europe and of the region of low pressure over Southern Europe. The wrongly-positioned and over-developed short-wave trough over the southern tip of Greenland is deepest in the 18-level hybrid forecast, and there is also a pronounced difference in the phase of the

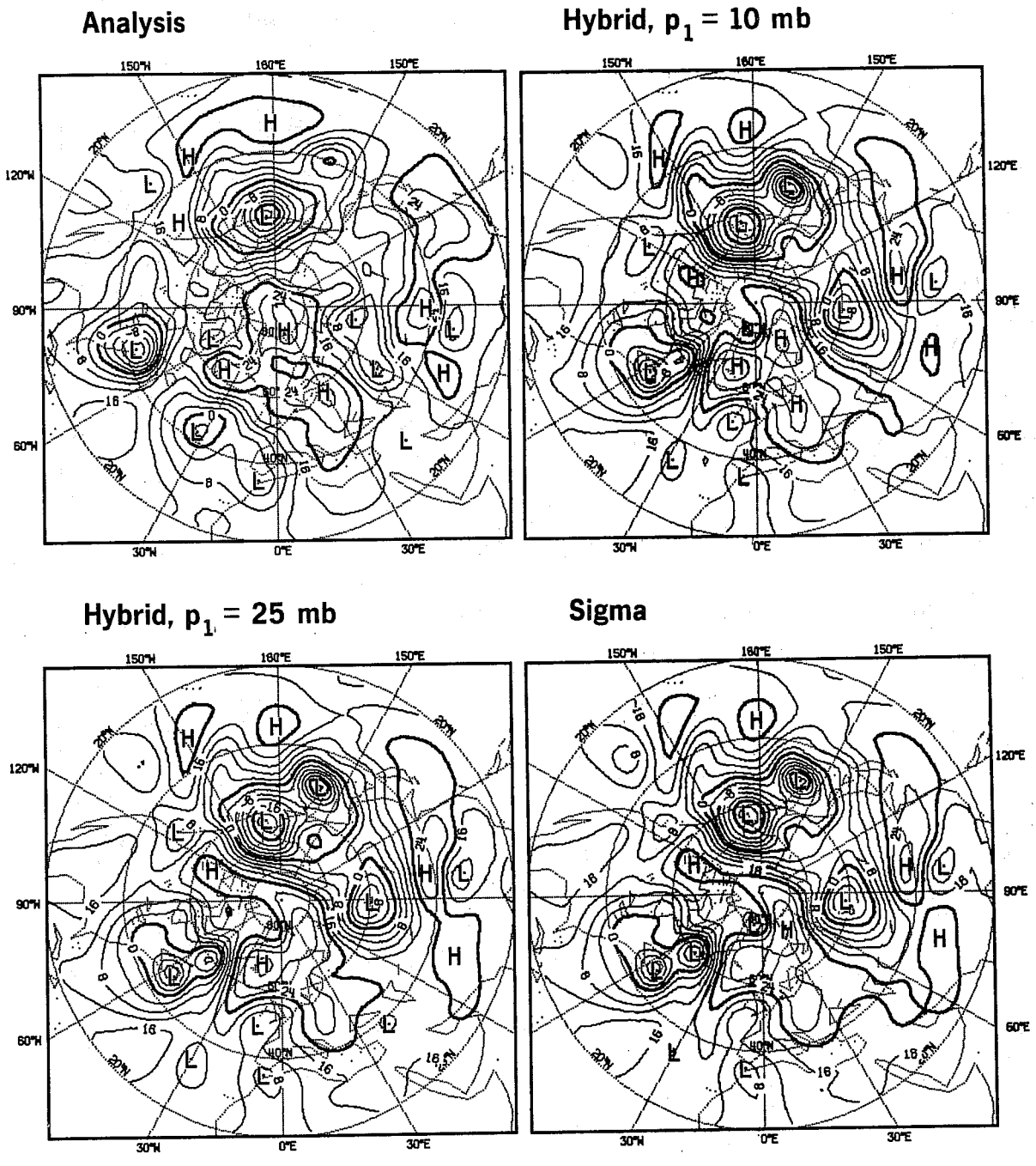

Fig. 11 The analysed 1000 mb height for the extratropical northern hemisphere for 22 January, 1979 (upper left) and corresponding 6-day forecasts from 16 January. The 18-level hybrid forecast is shown upper right and the sigma-coordinate forecast is lower right. The contour interval is 4 dam.

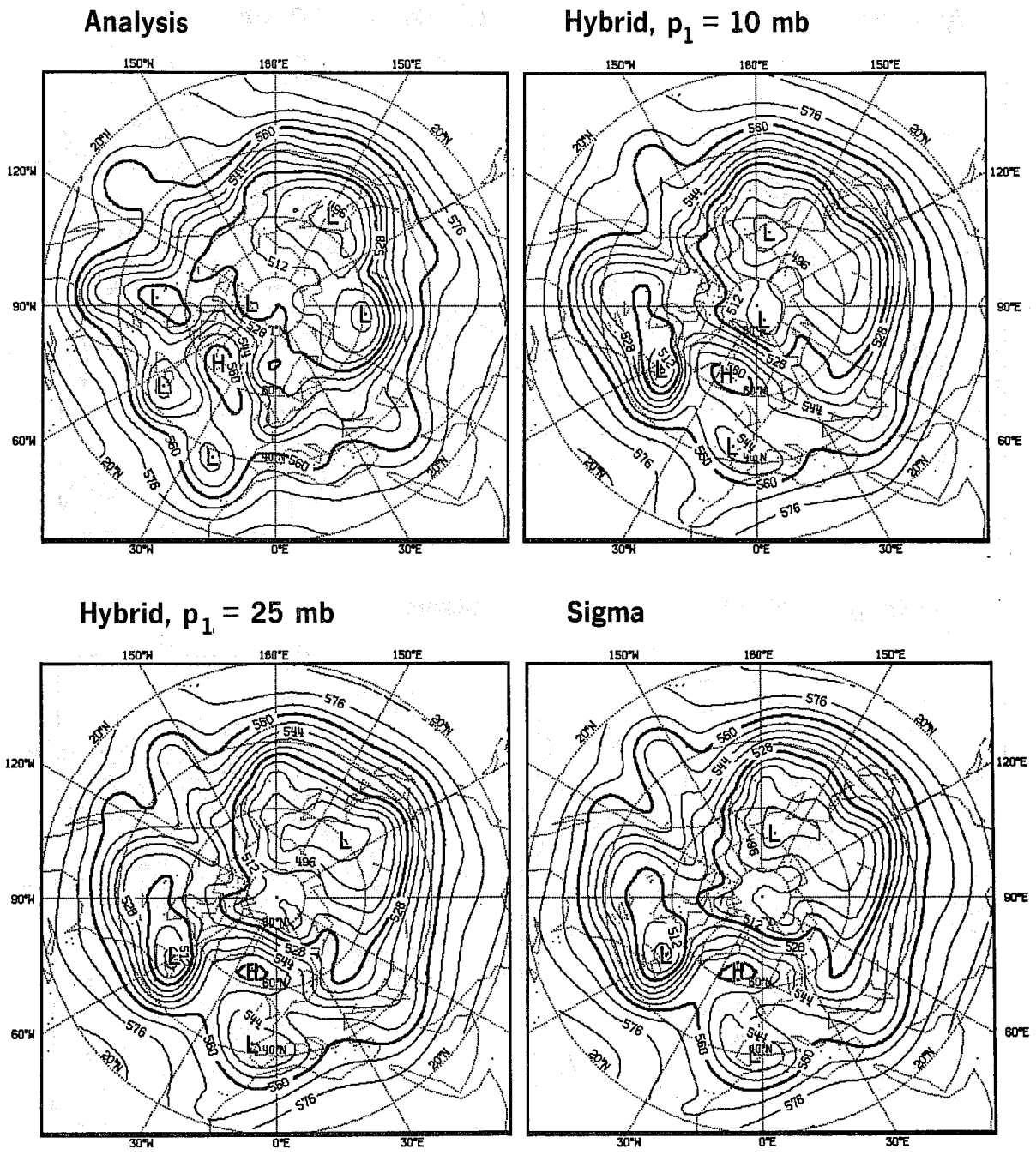

Fig. 12 As Figure 11 but for day 8 forecasts and the corresponding analysis, of the 500 mb height field. The contour interval is 8 dam.

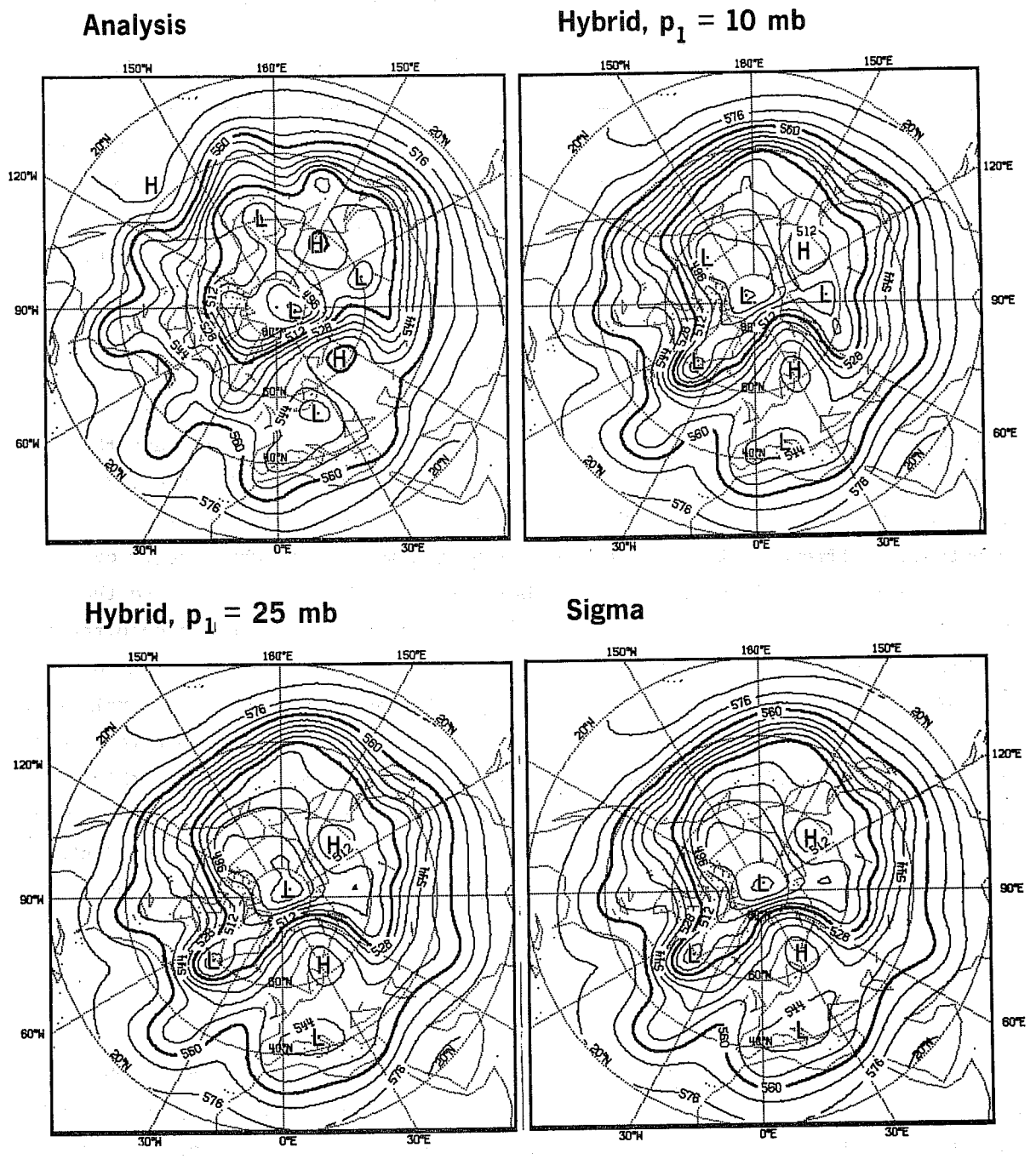

Fig. 13 As Figure 12, but for forecasts from 12 February, 1981.

trough over the Pacific, although all forecasts are so poor in this region that it is probably not meaningful to make comparisons with reality.

No systematic differences between the two coordinates and resolutions have been detected from examination of the mean height maps for the last five days of each forecast. Figure 14 shows for the 5 April case a characteristic model error of too deep a pressure over the North Atlantic and North Pacific Oceans. Small differences in maximum and minimum values can be seen, but the only major point to arise from examination of such maps is again the overall similarity of the forecasts of the height field.

A close examination of other aspects of forecast behaviour reveals some larger differences. A particular example is shown in Figure 15 which shows the convective precipitation accumulated over a portion of South America and the South-Eastern Pacific Ocean by day 4 of two forecasts from 16, January 1979. Over sea areas the two distributions are almost identical, but a quite substantial difference is found in the (high) maximum values which occur over the Andes mountain chain, lower values being found in the forecast using the hybrid coordinate. Subsequent experimentation has shown that such precipitation is highly sensitive to the so-called "horizontal" diffusion that is applied on model coordinate surfaces and which in its standard form acts to mix relatively warm low-level air with the relatively cold air that is located on mountain tops. The lower values of precipitation found with the hybrid coordinate probably reflect the more horizontal nature of coordinate surfaces away from lower levels, although the terrain-following nature of the coordinate at low levels evidently results in the problem being somewhat diminished rather than removed by use of the hybrid model.

12.3 Stratospheric forecasts

It has already been noted that marked circulation changes took place in the stratosphere during the 10-day periods following 16 January and 17 February 1979, and it is of interest to examine the forecasts of these events. The analyses of the 50 and 10mb heights for the two initial dates are presented in Figures 16 and 19, while day 4 and day 8 forecasts using the 18-level resolution and hybrid coordinate type 4 are compared with corresponding analyses in Figures 17, 18, 20 and 21.

Examination of these figures shows that in both cases the forecast model has successfully simulated a substantial breakdown of the circumpolar stratospheric circulation. Associated temperature rises in polar regions are also captured.

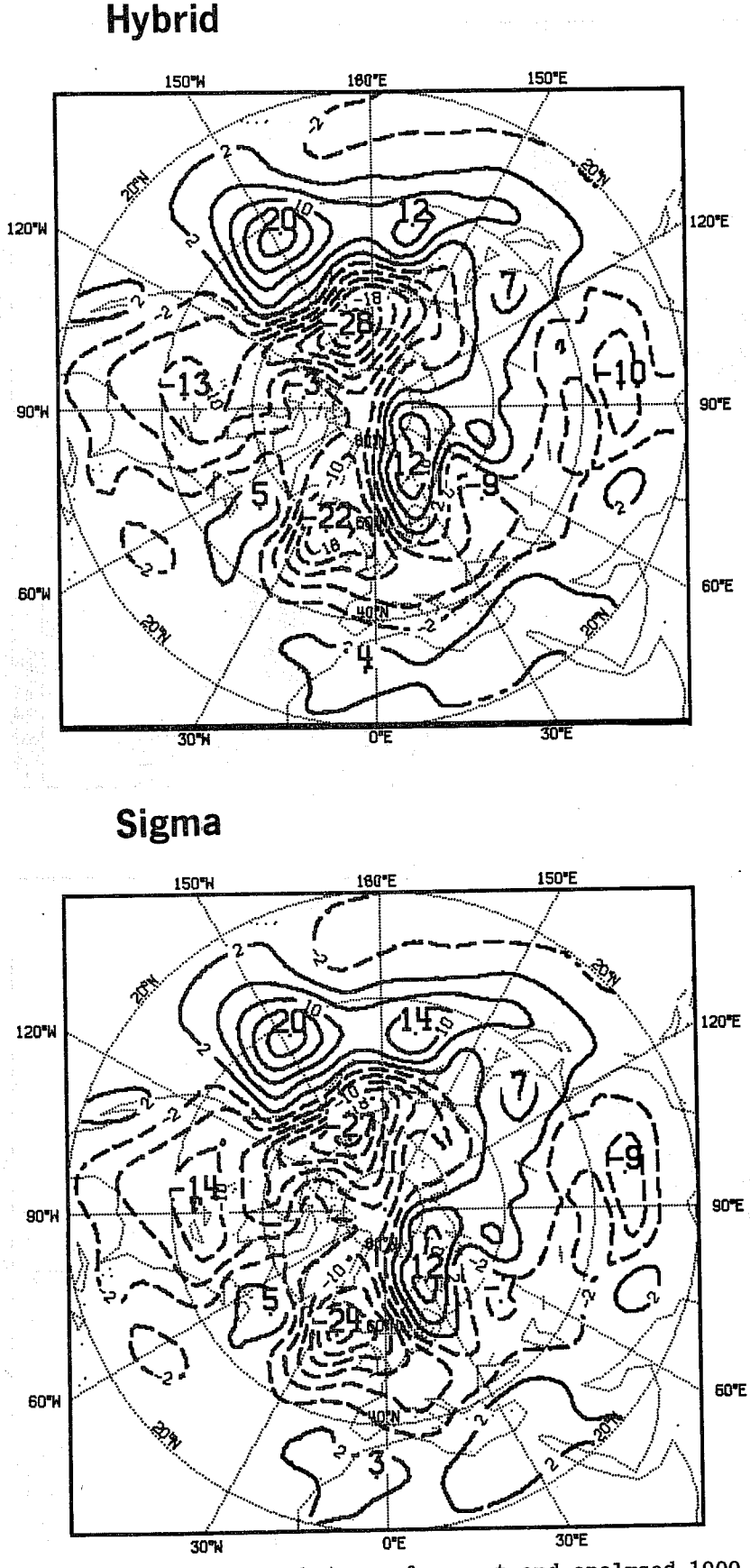

Fig. 14 Maps of the difference between forecast and analysed 1000 mb heights averaged over the last five days of the forecast from 5 April 1981. The upper plot is for the 18-level hybrid forecast using coordinate type 4, and the lower plot is for the sigma-coordinate forecast. The contour interval is 4 dam.

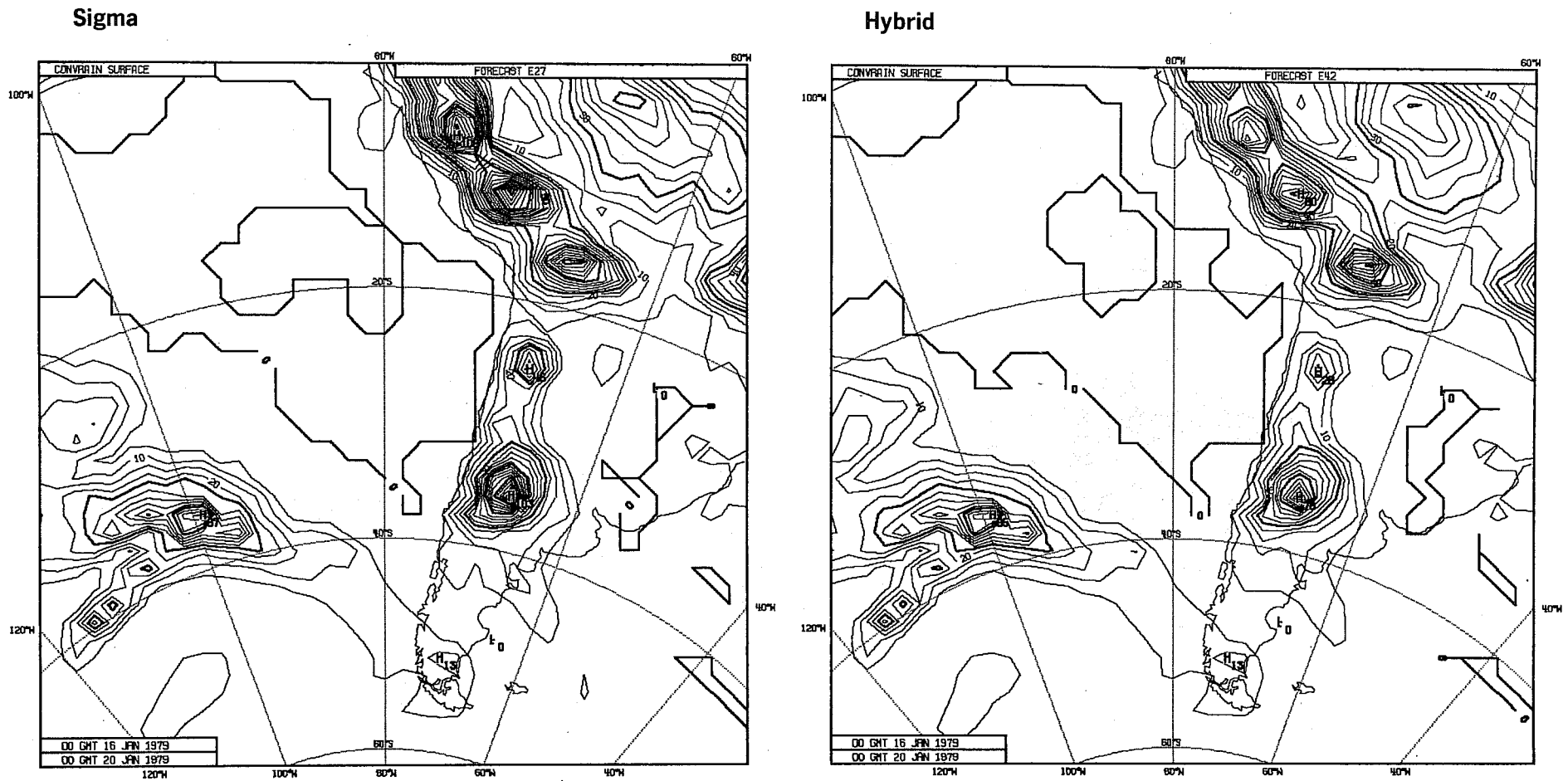

Fig. 15 Accumulated convective precipitation (mm) at day 4 of forecasts from 16 January 1979 for a region including part of South America. The hybrid forecast used co-ordinate type 4 and the 18-level resolution.

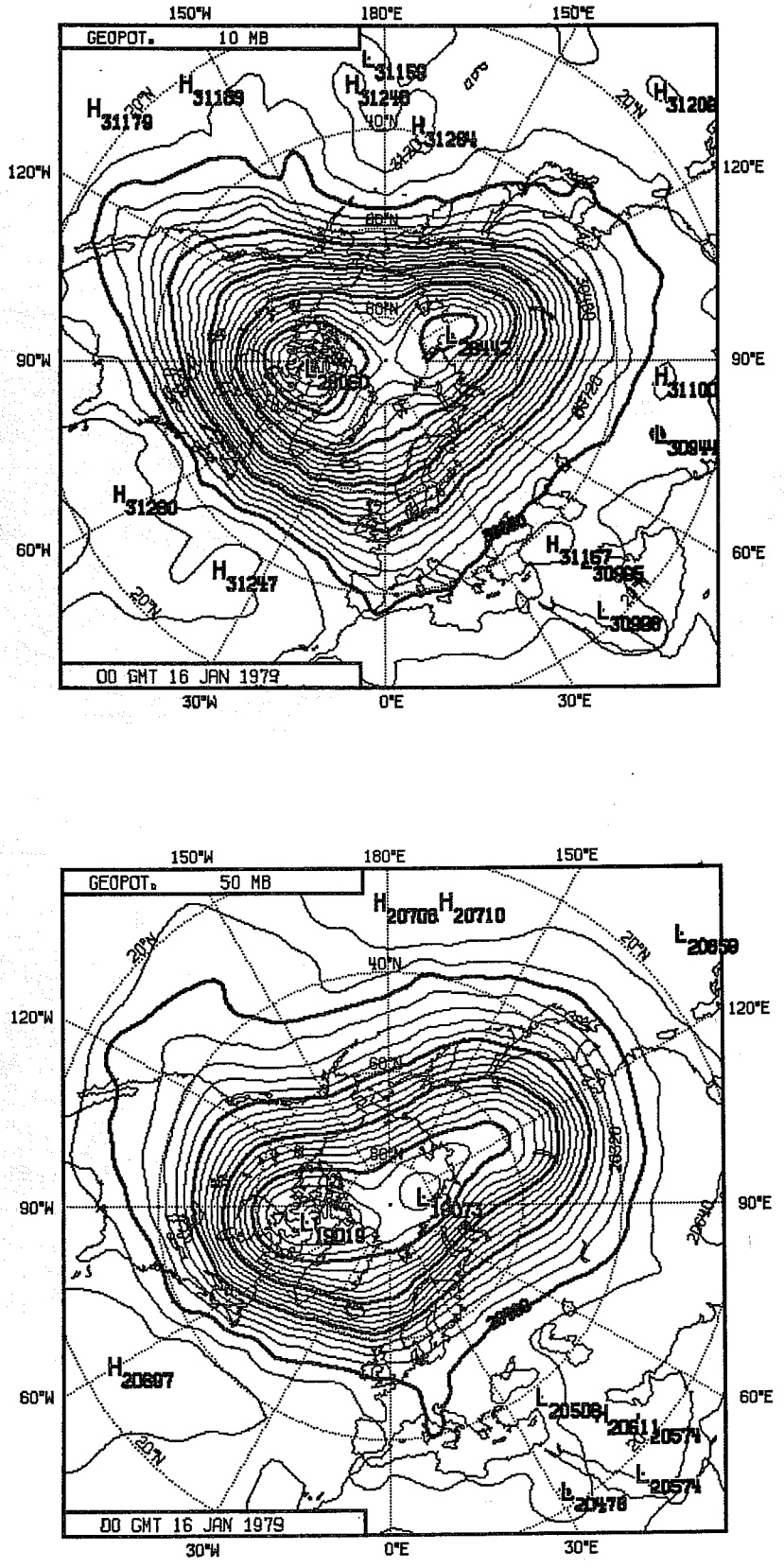

Fig. 16 10 mb (upper) and 50 mb (lower) analysed heights for 16 January 1979.

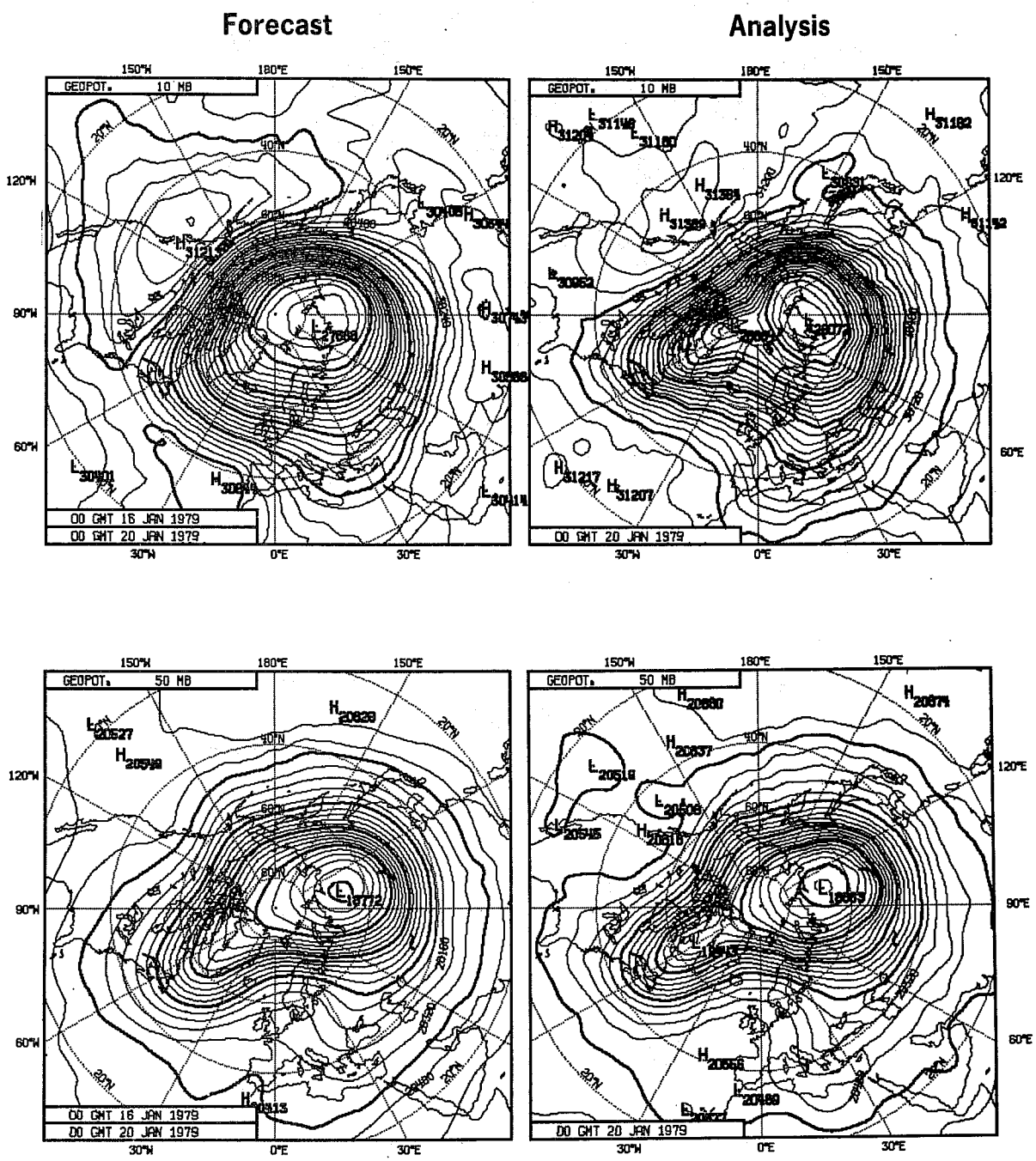

Fig. 17 Day 4 forecasts of 10 mb (upper) and 50 mb (lower) heights (left) and corresponding analyses (right) for the 16 January case.

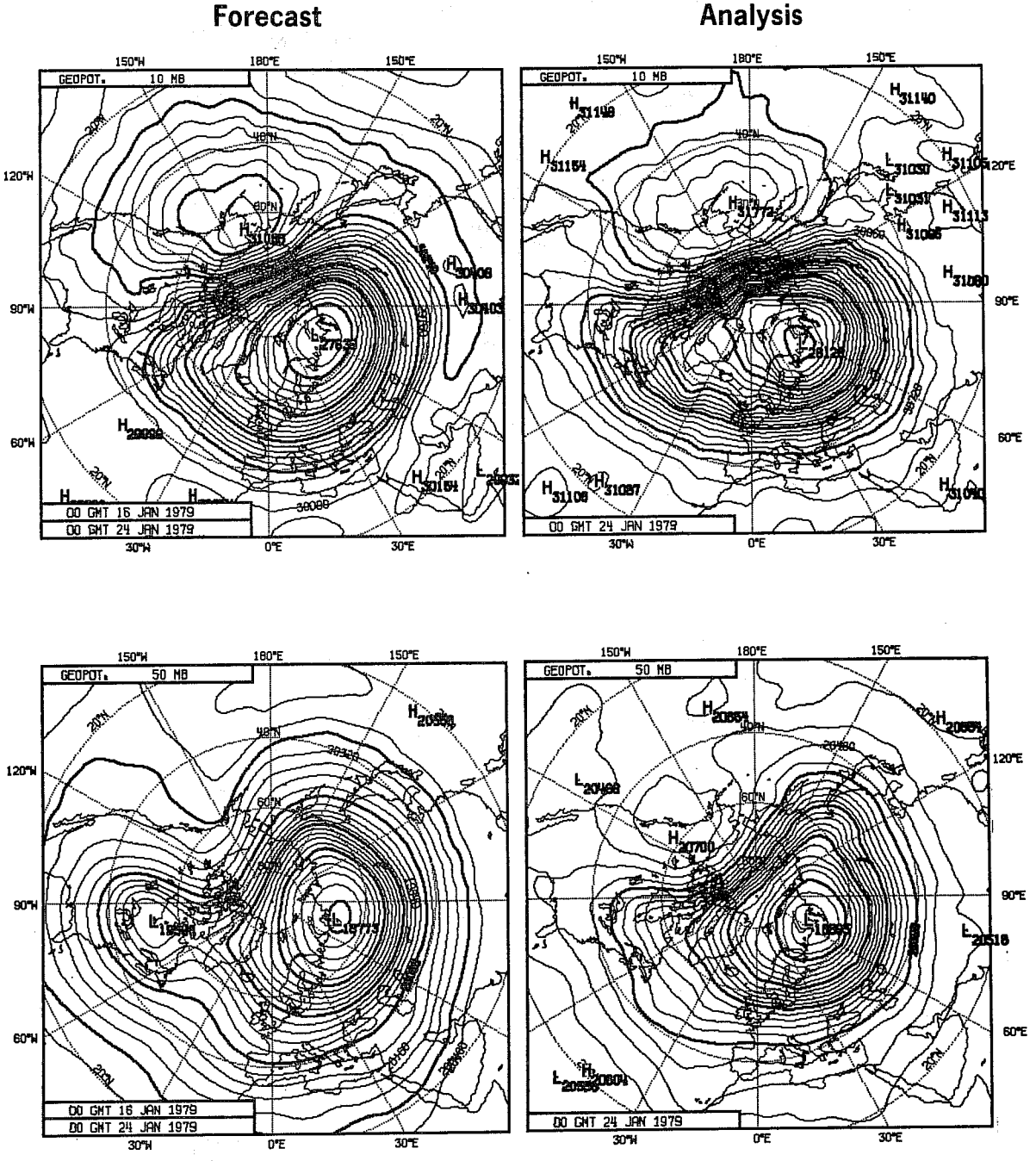

Fig. 18 As Figure 17, but for day 8.

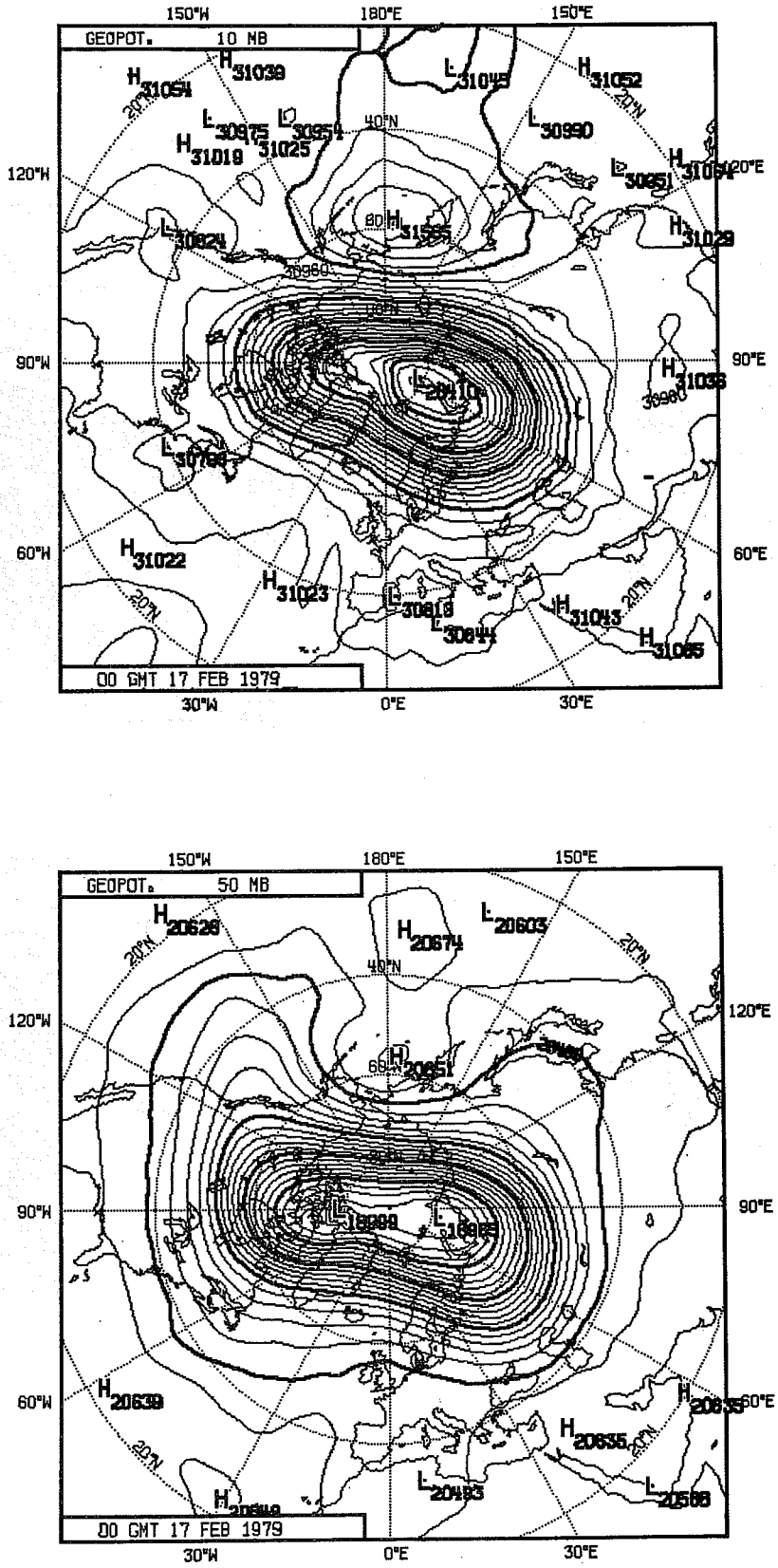

Fig. 19 10 mb (upper) and 50 mb (lower) analysed heights for 17 February 1979.

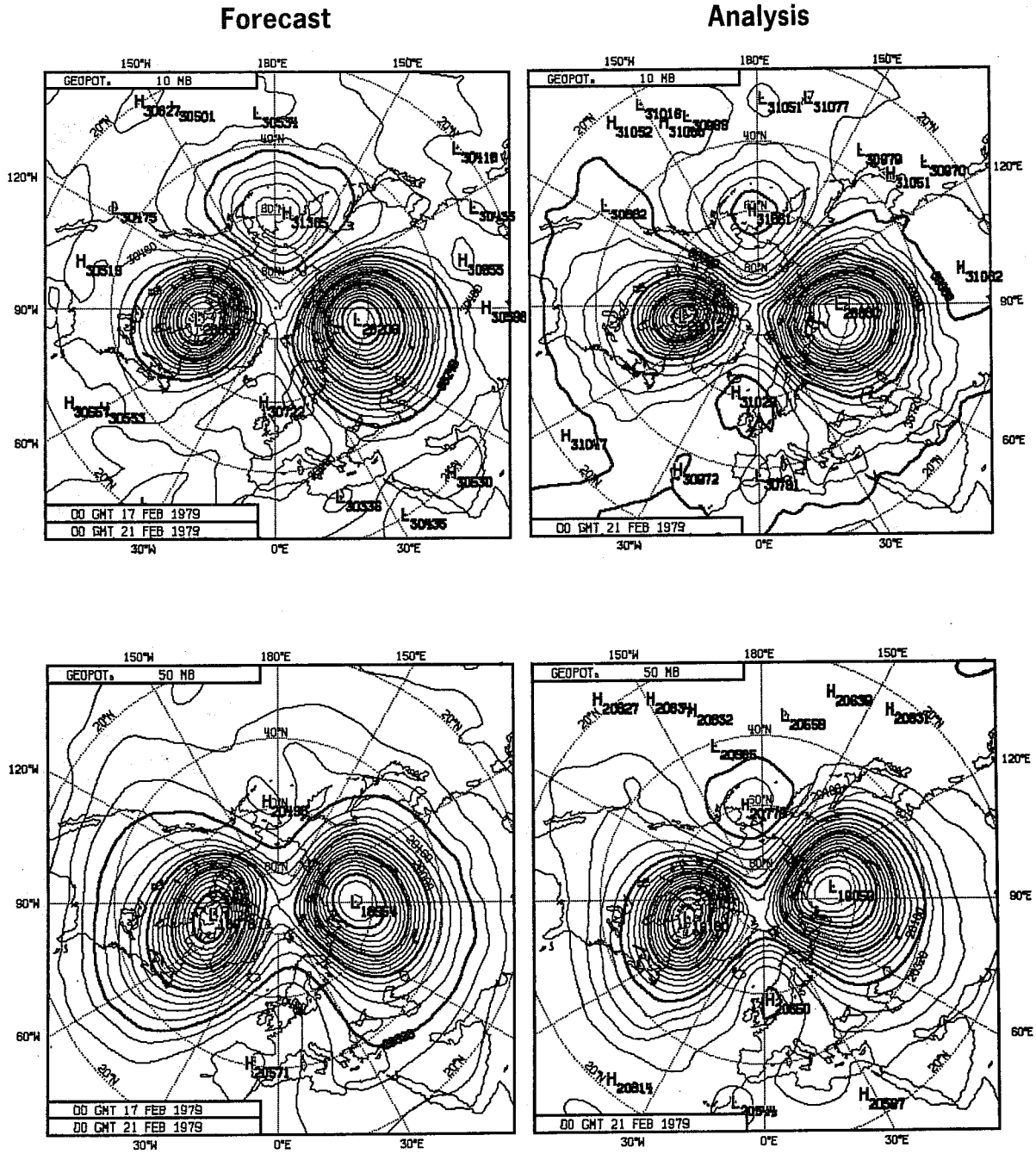

Fig. 20 As Figure 17, but for the 17 February case.

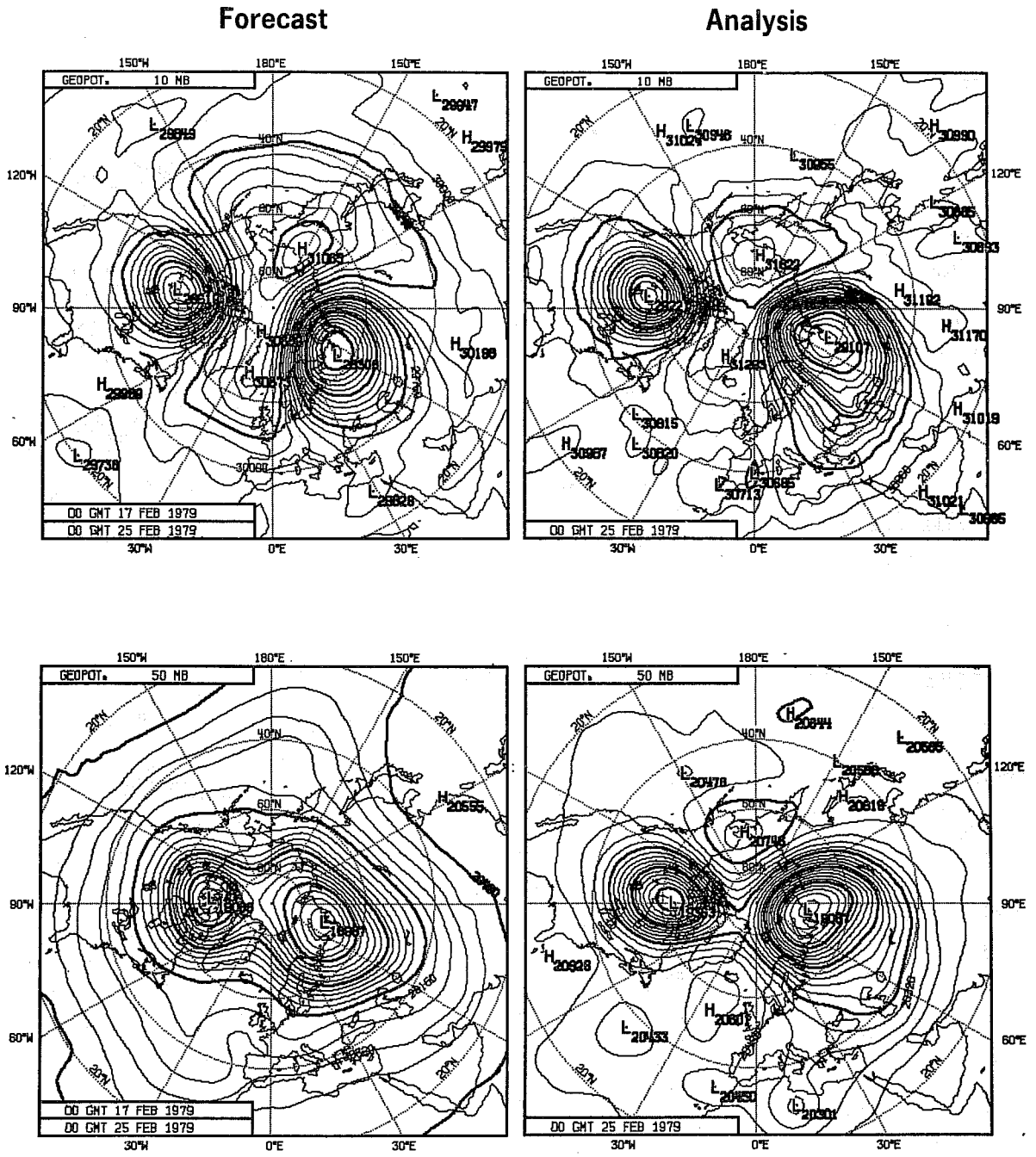

Fig. 21 As Figure 18, but for the 17 February case.

The wavenumber one breakdown which occurred in January is accurately represented at both 50 and 10mb for both days 4 and 8. For this forecast we have already commented on the high overall accuracy of the tropospheric forecast, and this accuracy is found to be pronounced in the larger scales of motion. The February breakdown occurs predominantly in zonal wavenumber two, and this too is very well simulated at day 4. By day 8 the 50mb forecast is clearly deficient, a deficiency which may be related to a poor tropospheric forecast of wavenumber two at this time, but the 10mb forecast still appears of good quality.

Another noteworthy feature of the stratospheric forecasts is that integrations performed with a top level at p = 25mb or σ = .025 generally give as accurate a 50mb forecast as the integrations with a 10mb top level. This is illustrated by plots of the amplitude and phase of the height perturbation at 60°N for wavenumber 1 (16 January forecast, Figure 22), and for wavenumber 2 (17 February forecast, Figure 23). Indeed, there is little evidence from these figures that forecasts are significantly deteriorated by a deficient upper boundary condition. The theoretical studies referenced in section 9 suggest that such a deficiency would manifest itself in a spuriously-reflected downward-propagating planetary-wave component, leading to phase lines which would show less of a westward phase tilt with height. There is no clear sign of this in Figures 22 and 23, the 18-level forecasts giving particularly accurate representations of phase up to the 10mb level, although there is some indication of too large a wave amplitude at the topmost level. Only towards the end of the February forecast is some benefit from a 10mb top level seen in the lower stratosphere, an improved phase structure giving the substantially improved eddy heat flux shown in Figure 24.

12.4 The traditional hybrid coordinate

Preliminary tests of the implementation of the general finite-difference scheme into the forecast model used an N24 horizontal resolution and the 15-level resolution used for the idealized tests described in this report. A sigma-coordinate forecast from 16 January, 1979 was compared with one using hybrid coordinate type 3 and with one using the traditional hybrid coordinate with an interfacial pressure of 105mb (type 2a). Results showed the traditional hybrid coordinate to give a forecast slightly better than that given by the sigma coordinate but slightly worse than that given by coordinate type 3. Subsequent tests of coordinate type 2 using the N48 horizontal resolution revealed problems of computational stability as suggested by the idealized analysis discussed in section 8. Forecasts from 16 January, 1979 and 17 February,

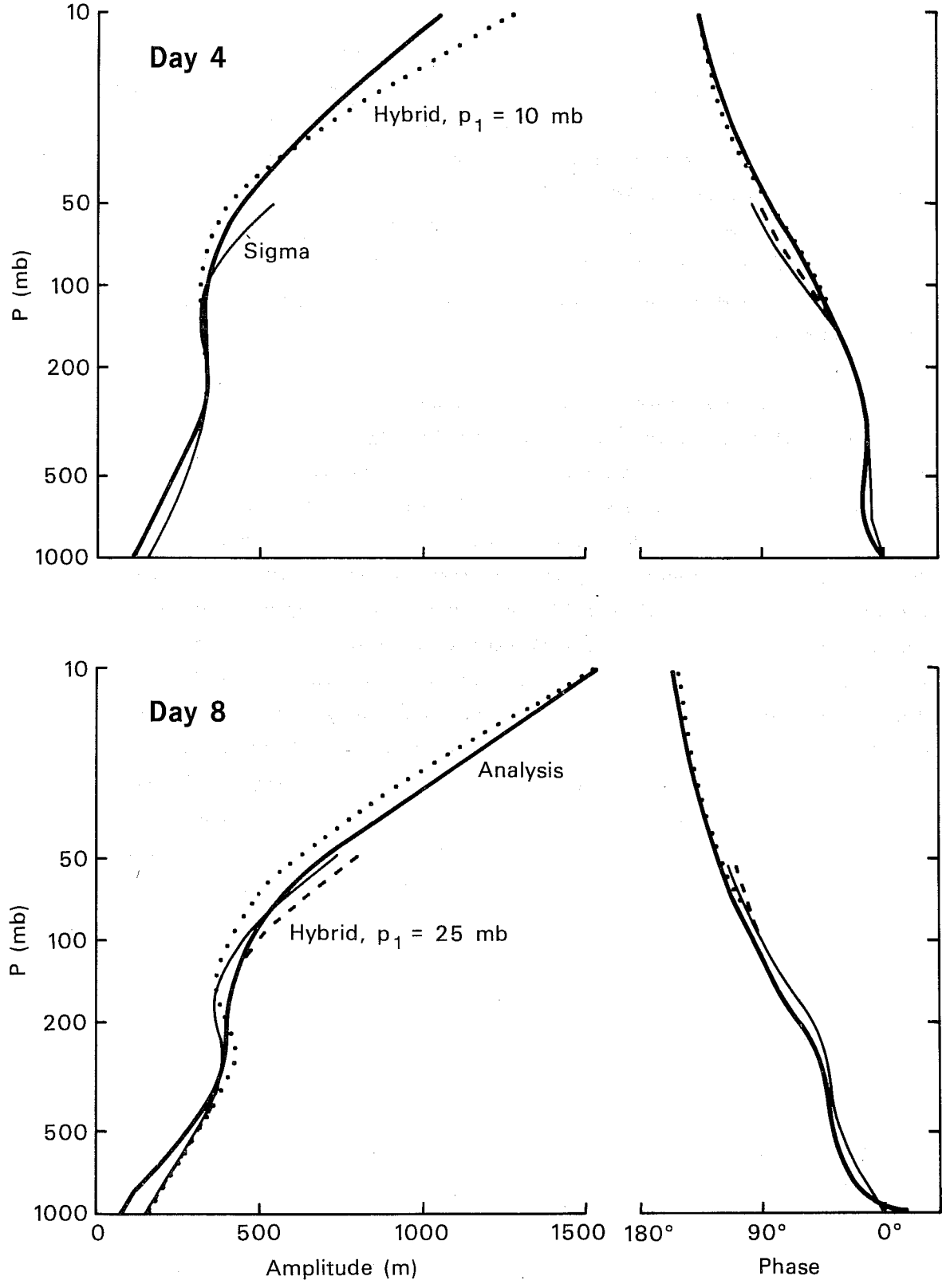

Fig. 22 The amplitude and phase of the zonal wavenumber one component of the height field at 60°N for day 4 and day 8 of the forecasts from 16 January, 1979. The heavy solid line refers to the analysis, the light solid line to the sigma-coordinate forecast, the dotted line to the 18-level hybrid forecast using coordinate type 4 and the dashed line to the corresponding 16-level hybrid forecast. The latter two lines are not drawn where they are indistinguishable from the sigma-coordinate curves.

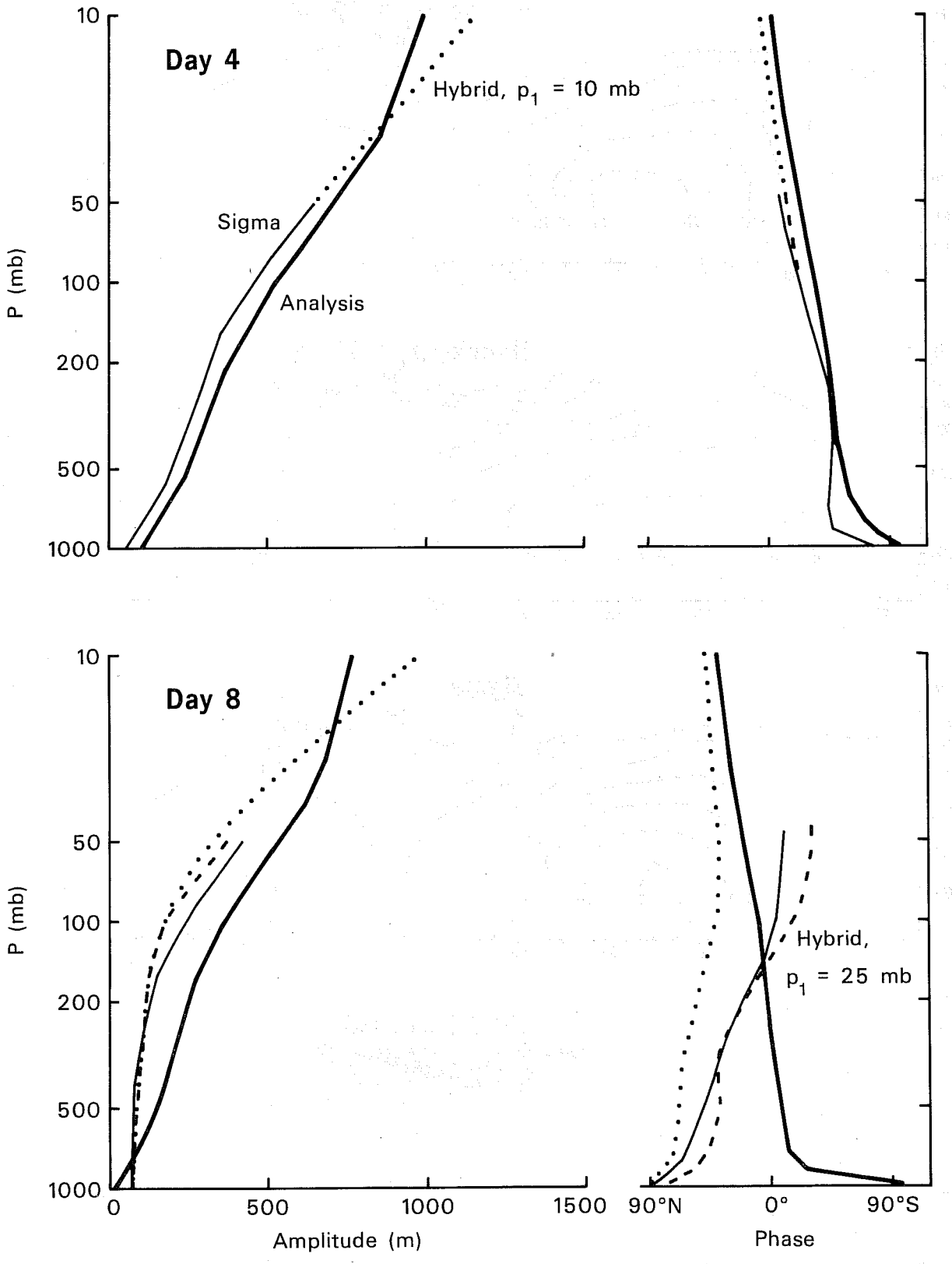

Fig. 23 As Figure 22 but for zonal wavenumber 2 and the 17 February forecasts.

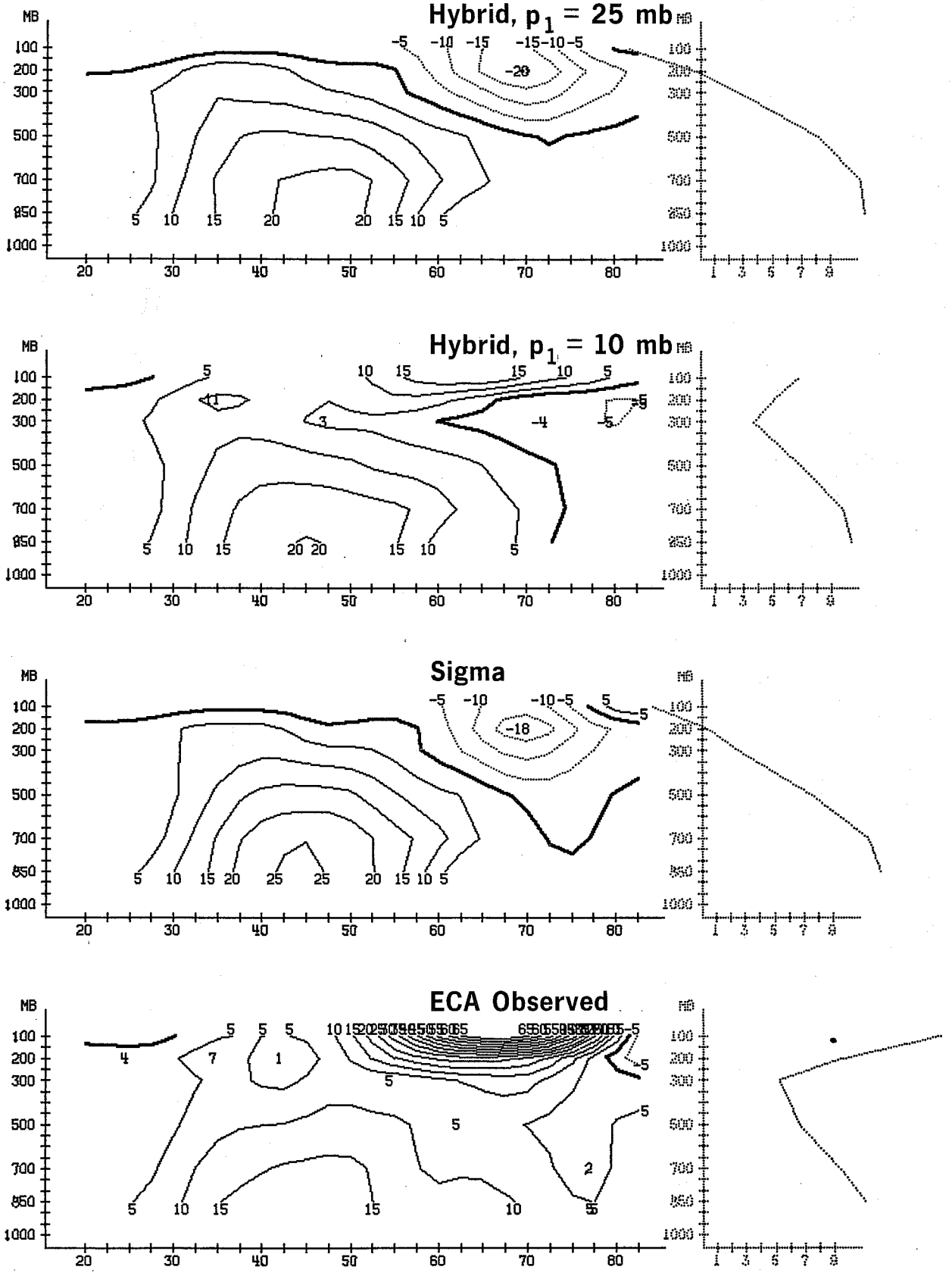

Fig. 24 The eddy heat flux (Kms^{-1}) averaged over the last five days of forecasts from 17 February, and corresponding analysed values. The hybrid forecasts used coordinate type 4.

1979 using the 18-level resolution illustrated in Figure 1 both became unstable after about 5 days of integration using a reference surface pressure of 1013.2 mb. Further integrations on the 16 January case showed the instability to occur also with a reference pressure of 800mb, and with a warmer isothermal reference temperature of 400 K.

In view of these results, further experimentation with this coordinate has not been carried out.

12.5 Other results

The integrations reported here using hybrid coordinate type 3 used a reference surface pressure of 1013.2mb for the semi-implicit scheme, and all such integrations have been found to be computationally stable. Computational instability was, however, encountered for this reference pressure in the first (18-level) forecast performed using coordinate 4. Changing the reference surface pressure to 800mb stabilized this integration, and all subsequent integrations using this reference value and coordinate 4 have been found to be stable. The overall insensitivity of forecast quality to the choice of either coordinate type 3 or coordinate type 4, as shown in Figure 7, indicates that provided stable integration is achieved the choice of reference pressure is of little consequence.

An integration has also been performed for the 16 January case to compare, for the sigma coordinate, the vertical finite-difference scheme used operationally at ECMWF with the modified scheme adopted for the other integrations reported here. This comparison revealed negligible differences up to day 8. A very small advantage in favour of the operational scheme was found beyond this time, but significance should not be attached to such differences(which are smaller than shown in Figure 6) towards the end of just one forecast of anomalous quality.

13. CONCLUDING REMARKS

We have introduced an energy and angular momentum conserving vertical finite-difference scheme for a general terrain-following vertical coordinate wich is a function of pressure and its surface value. For an appropriate definition of full-level pressure the error in the pressure gradient over steep orography vanishes for a logarithmic temperature profile in the special case of sigma coordinates. The formulation of the finite-difference scheme is such that a change of vertical coordinate requires only a change in the calculation of half-level values of pressure and its derivative with respect to surface pressure.

With careful design the computational cost of including this flexibility in a model is unlikely to be large.

Estimates of the error in the pressure gradient over steep orography indicate generally small tropospheric values, but large sigma-coordinate errors above a sharp tropopause. These errors are partially reduced for the traditional hybrid vertical coordinate when the interface above which the coordinate reduces to pressure is located in the stratosphere, and substantially reduced when the interface is located just below the tropopause. In the latter case, however, the semi-implicit time scheme is less stable over high orography, and a spurious gravitational instability may occur below the interface. A compromise between computational stability and the accuracy of the stratospheric pressure gradient may be found with the alternative hybrid coordinates introduced in section 5.

The forecast experiments show that the overall quality of forecasts is largely insensitive to the choice of vertical coordinate. Such differences as have been found generally favour the use of a hybrid coordinate, although caution must of course be exercised in drawing conclusions from the results of just four cases. It is important to note that in these experiments the hybrid coordinates were not incorporated into the forecast model used in data assimilation cycles. There seems little doubt that use of such coordinates would facilitate the design and implementation of a data assimilation system in which the analysis itself is performed on pressure surfaces, although it is difficult to assess in advance the resulting impact on the accuracy of the forecasts.

Tropospheric sensitivity to raising the top model level from 25 to 10mb is seen clearly only towards the end of the 10-day forecast period, and since only two of the cases studied exhibited useful skill at such times it is difficult to draw firm conclusions concerning the importance of stratospheric resolution. Study of the forecasts of stratospheric warming events indicates that limited upper-level resolution does not inhibit the accurate prediction of major circulation changes. In particular, the accuracy of the forecasts close to the top model level suggests that events in the upper (unresolved) stratosphere played only a minor rôle in the dynamics of the warmings studied, although the possibility of fortuitous results due to a cancellation of model errors cannot be ruled out entirely.

It is not within the scope of this report to make specific recommendations concerning the choice of vertical coordinate. In practice the best choice will very much depend on the purpose for which the primitive equation model is to be used, the vertical resolution that can be employed, and the type of orography used. Studies such as that reported here may help guide this choice. Regarding the specific field of numerical weather prediction there is no evidence to

justify a sudden change of an existing operational model from sigma to hybrid coordinates, but it would appear to be advisable to allow for the possible use of hybrid coordinates by a flexible design of any new forecasting system that is to be based on use of a terrain-following vertical coordinate. Such a course is being followed in the preparation of a new system at ECMWF.

Acknowledgements.
We are very grateful to D.M. Burridge for suggesting this study and for his subsequent interest and advice. Thanks are also due to M. Jarraud for stimulating discussions on alternative forms of hybrid coordinate, and to many other members of the Research Department at ECMWF for advice on points of detail. Comments by A. Hollingsworth and F. Mesinger on a draft of this report are acknowledged with thanks.

REFERENCES

Arakawa, A. and V.R. Lamb, 1977: Computational design of the basic dynamical processes of the UCLA general circulation model. Methods in Computational Physics, Vol. 17, J. Chang, Ed., Academic Press, 337pp.

Bates, J.R., 1977: Dynamics of stationary, ultra-long waves in middle latitudes. Quart. J. Roy. Meteor. Soc., 103, 397-430.

Bengtsson, L., 1981: Numerical prediction of atmospheric blocking - A case study. Tellus, 33, 19-42

Burridge, D.M. and J. Haseler, 1977: A model for medium range weather forecasting - Adiabatic formulation. ECMWF Technical Report No. 4, 46pp.

Charney, J.G., 1947: The dynamics of long-waves in a baroclinic westerly current. J. Meteor., 4, 135-162.

Corby, G.A., A. Gilchrist and R.L. Newson, 1972: A general circulation model of the atmosphere suitable for long period integration. Quart. J. Roy. Meteor. Soc., 98, 809-832.

Desmarais, J-G. and J. Derome, 1978: Some effects of vertical resolution on modelling forced planetary waves with a time-dependent model. Atmosphere-Ocean, 16, 212-225.

Fels, S.B., J.D. Mahlman, M.D. Schwarzkopf and R.W. Sinclair, 1980: Stratospheric sensitivity to perturbations in ozone and carbon dioxide: Radiative and dynamical response. J. Atmos. Sci., 37, 2265-2297

Gary, J.M., 1973: Estimate of truncation error in transformed coordinate, primitive equation atmospheric models, J. Atmos. Sci., 30, 223-233.

Girard, C. and M. Jarraud, 1981: Comparison of Medium Range Forecasts made with models using spectral or finite difference techniques in the horizontal. To appear as an ECMWF Technical Report.

Hoskins, B.J. and A.J. Simmons, 1975: A multi-layer spectral model and the semi-implicit method. Quart. J. Roy. Meteor. Soc., 101, 637-655.

Kasahara, A., 1974: Various vertical coordinate systems used for numerical weather prediction. Mon. Wea. Rev., 102, 509-522.

Kirkwood, E. and J. Derome, 1977: Some effects of the upper boundary condition and vertical resolution on modelling forced stationary planetary waves. Mon. Wea. Rev., 105, 1239-1251.

Lindzen, R.S. E.S. Batten and J.W. Kim, 1968: Oscillations in atmospheres with tops. Mon. Wea. Rev., 96, 133-140.

Mesinger, F., 1981: On the convergence and error problems of the calculation of the pressure gradient force in sigma coordinate models. To appear in Geophys. Astrophys. Fluid. Dynam.

Nakamura, H., 1976: Some problems in reproducing planetary waves by numerical models of the atmosphere. J. Meteor. Soc. Japan, 54, 129-146.

Nakamura, H., 1978: Dynamical effects of mountains on the general circulation of the atmosphere: I. Development of finite-difference schemes suitable for incorporating mountains. J. Meteor. Soc. Japan, 56,317-339.

Phillips, N.A., 1957: A coordinate system having some special advantages for numerical forecasting. J. Meteor., 14, 184-185.

Sangster, W.E. 1960: A method of representing the horizontal pressure force without reduction of station pressures to sea level. J. Meteor., 17, 166-176.

Schlesinger, M.E. and Y. Mintz, 1979: Numerical simulation of ozone production transport and distribution with a global atmospheric general circulation model. J. Atmos. Sci., 36, 1325-1361.

Simmons, A.J. and B.J. Hoskins, 1976: Baroclinic instability on the sphere: Normal modes of the primitive and quasi-geostrophic equations. J. Atmos. Sci., 33, 1454-1477.

Simmons, A.J., B.J. Hoskins and D.M. Burridge, 1978: Stability of the semi-implicit time scheme. Mon. Wea. Rev., 106, 405-412.

Sundqvist, H., 1976: On vertical interpolation and truncation in connexion with use of sigma system models. Atmosphere, 14, 37-52.

White, A.A., 1977: Modified quasi-geostrophic equations using geometric height as vertical coordinate. Quart. J. Roy. Meteor. Soc., 103, 383-396.

APPENDIX A - THE CONSERVATION OF ANGULAR MOMENTUM

The vertically integrated pressure gradient force is given in continuous form by

$$\int_0^1 \frac{\partial p}{\partial \eta} \{ \nabla\phi + \frac{RT}{p} \nabla p \} d\eta$$

$$= \int_0^1 \frac{\partial p}{\partial \eta} \{ \nabla\phi - \frac{1}{\partial p/\partial \eta} \frac{\partial \phi}{\partial \eta} \nabla p \} d\eta \text{ , by the hydrostatic relation,}$$

$$= \int_0^1 \frac{\partial p}{\partial \eta} \nabla\phi d\eta - \int_0^1 (\nabla p) \frac{\partial \phi}{\partial \eta} d\eta$$

$$= \int_0^1 \frac{\partial p}{\partial \eta} \nabla\phi d\eta - \phi_s \nabla p_s + \int_0^1 \phi \nabla \frac{\partial p}{\partial \eta} d\eta \text{, using integration by parts,}$$

$$= \nabla \int_0^1 \phi \frac{\partial p}{\partial \eta} d\eta - \phi_s \nabla p_s \text{ .}$$

Integrating the zonal component of this expression round a latitude circle shows the net contribution to the change of angular momentum due to the pressure gradient to be given by a "mountain torque" term proportional to $\int \phi_s (\partial p_s / \partial \lambda) d\lambda$

This result holds for the finite-difference scheme provided

$$\sum_{k=1}^{NLEV} \{ \frac{\partial \phi_k}{\partial \lambda} \Delta p_k + R \left(\frac{T}{p} \frac{\partial p}{\partial \lambda} \right)_k \Delta p_k \} = \frac{\partial}{\partial \lambda} \sum_{k=1}^{NLEV} \phi_k \Delta p_k - \phi_s \frac{\partial p_s}{\partial \lambda} \text{ ,}$$

i.e. provided that

$$\sum_{k=1}^{NLEV} R \left(\frac{T}{p} \frac{\partial p}{\partial \lambda} \right)_k = \sum_{k=1}^{NLEV} \phi_k \frac{\partial}{\partial \lambda} \Delta p_k - \phi_s \frac{\partial p_s}{\partial \lambda}$$

Using the relations

$$\phi_k = \phi_{k+\frac{1}{2}} + \alpha_k RT_k \text{ ,}$$

$$\phi_{k+\frac{1}{2}} = \phi_s + \sum_{j=k+1}^{NLEV} RT_j \ell n \frac{p_{j+\frac{1}{2}}}{p_{j-\frac{1}{2}}} \text{ ,}$$

and $$\sum_{k=1}^{NLEV} \Delta p_k = p_s \text{ ,}$$

this condition may be written

$$\sum_{k=1}^{NLEV} R \left(\frac{T}{p} \frac{\partial p}{\partial \lambda} \right)_k \Delta p_k = \sum_{k=1}^{NLEV} \{ \alpha_k RT_k + \phi_{k+\frac{1}{2}} \} \frac{\partial}{\partial \lambda} (\Delta p_k) - \phi_s \frac{\partial p_s}{\partial \lambda}$$

$$= \sum_{k=1}^{NLEV} R \{ \frac{\alpha_k T_k}{\Delta p_k} \frac{\partial}{\partial \lambda} (\Delta p_k) \} \Delta p_k$$

$$+ \sum_{k=1}^{NLEV} \sum_{j=k+1}^{NLEV} RT_j \ell n \frac{p_{j+\frac{1}{2}}}{p_{j-\frac{1}{2}}} \frac{\partial}{\partial \lambda} (\Delta p_k) \text{ .}$$

Rearranging the double sum gives the requirement

$$\sum_{k=1}^{NLEV} R\left(\frac{T}{p}\frac{\partial p}{\partial \lambda}\right)_k \Delta p_k = \sum_{k=1}^{NLEV} \left\{ \frac{RT_k}{\Delta p_k} \left[\left(\ell n \frac{p_{k+\frac{1}{2}}}{p_{k-\frac{1}{2}}}\right) \sum_{j=1}^{k-1} \frac{\partial}{\partial \lambda}(\Delta p_j) + \right.\right.$$

$$\left.\left. + \alpha_k \frac{\partial}{\partial \lambda}(\Delta p_k) \right] \right\} \Delta p_k ,$$

and, since $\sum_{j=1}^{k-1} \Delta p_j = p_{k-\frac{1}{2}}$, this is clearly satisfied by the form (3.8) chosen for the pressure gradient term.

APPENDIX B - MATRICES AND VECTORS FOR THE SEMI-IMPLICIT SCHEME

The matrices and vectors introduced in section 4 are given by

$$(\underset{\approx}{\gamma})_{jk} = 0 \quad , k < j \ ,$$

$$= R\alpha_k \ , \ k=j,$$

$$= R\ell n \frac{p_{k+\frac{1}{2}}}{p_{k-\frac{1}{2}}} \quad , k > j \ ;$$

$$(\underset{\approx}{\tau})_{jk} = \frac{\Delta p_k}{\Delta p_j} \kappa T_{rj} (\underset{\approx}{\gamma})_{kj} + \frac{1}{2\Delta p_j} \{$$

$$(T_{r(j+1)} - T_{rj}) \left(\frac{\partial p}{\partial p_s}\right)_{j+\frac{1}{2}} \Delta p_k - \begin{vmatrix} 0 \ , & k > j, \\ \Delta p_k, & k \leq j, \end{vmatrix}$$

$$+ (T_{rj} - T_{r(j-1)}) \left(\frac{\partial p}{\partial p_s}\right)_{j-\frac{1}{2}} \Delta p_k - \begin{vmatrix} 0 & ,(k+1) > j, \\ \Delta p_k & ,(k+1) \leq j, \end{vmatrix} \} \ ;$$

$$(\underset{\sim}{\nu})_j = \Delta p_j \ ;$$

$$(\underset{\sim}{h}_1)_j = \frac{RT_{rj}}{\Delta p_j} \{ (\ell n \frac{p_{j+\frac{1}{2}}}{p_{j-\frac{1}{2}}}) \left(\frac{\partial p}{\partial p_s}\right)_{j-\frac{1}{2}} + \alpha_j \left[\left(\frac{\partial p}{\partial p_s}\right)_{j+\frac{1}{2}} - \left(\frac{\partial p}{\partial p_s}\right)_{j-\frac{1}{2}} \right] \};$$

$$(\underset{\sim}{h}_2)_j = RT_{rj} \frac{\partial \alpha_j}{\partial p_s} + \sum_{k=j+1}^{NLEV} RT_{rk} \{ \frac{1}{p_{k+\frac{1}{2}}} \left(\frac{\partial p}{\partial p_s}\right)_{k+\frac{1}{2}} - \frac{1}{p_{k-\frac{1}{2}}} \left(\frac{\partial p}{\partial p_s}\right)_{k-\frac{1}{2}} \}.$$

If $\alpha_j = 1 - \frac{p_{j-\frac{1}{2}}}{\Delta p_j} \ell n \frac{p_{j+\frac{1}{2}}}{p_{j-\frac{1}{2}}}$

then $\partial \alpha_j / \partial p_s$ may readily be expressed as a function of $(\partial p/\partial p_s)_{j-\frac{1}{2}}$ and $(\partial p/\partial p_s)_{j+\frac{1}{2}}$. In this case we find

$$(\underset{\sim}{h}_1 + \underset{\sim}{h}_2)_j = \frac{RT_{rj}}{p_{j+\frac{1}{2}}} \left(\frac{\partial p}{\partial p_s}\right)_{j+\frac{1}{2}} + \sum_{k=j+1}^{NLEV} RT_{rk} \left\{ \frac{1}{p_{k+\frac{1}{2}}} \left(\frac{\partial p}{\partial p_s}\right)_{k+\frac{1}{2}} - \frac{1}{p_{k-\frac{1}{2}}} \left(\frac{\partial p}{\partial p_s}\right)_{k-\frac{1}{2}} \right\}.$$

All expressions are evaluated at the reference surface pressure, p_r.

APPENDIX C - SOME DETAILS OF THE FORMULATION OF THE QUASI-GEOSTROPHIC MODEL

As in section 4 we represent variables at each of the NLEV levels of the model by column vectors, and take an initial state with horizontal-mean temperature $\underset{\sim}{T}_r$, zonal-mean temperature gradient $\overline{\underset{\sim}{T}}_y$, pressure gradient $\overline{p}_{sy}$, and zonal mean flow $\overline{\underset{\sim}{u}}$. Linear balance gives

$$f\overline{\underset{\sim}{u}} = -\underset{\approx}{\gamma}\,\overline{\underset{\sim}{T}}_y - (\underset{\sim}{h}_1 + \underset{\sim}{h}_2)\,\overline{p}_{sy} \qquad (C.1)$$

where $\underset{\approx}{\gamma}$, $\underset{\sim}{h}_1$ and $\underset{\sim}{h}_2$ are as defined in Appendix B.

The perturbation stream function, divergence, temperature and surface pressure are represented by complex amplitudes $\underset{\sim}{\psi}'$, $\underset{\sim}{D}'$, $\underset{\sim}{T}'$ and p_s' respectively, and satisfy the equations

$$\frac{\partial}{\partial t}\underset{\sim}{\psi}' - \frac{f}{k^2}(\underset{\sim}{D}' + \underset{\approx}{M}_1\underset{\sim}{\psi}') + \underset{\approx}{M}_2\underset{\sim}{T}' + \underset{\sim}{N}_1 p_s' = 0 \qquad (C.2)$$

$$\frac{\partial}{\partial t}\underset{\sim}{T}' + \underset{\approx}{\tau}\underset{\sim}{D}' + \underset{\approx}{M}_3\underset{\sim}{\psi}' + \underset{\approx}{M}_4\underset{\sim}{T}' + \underset{\sim}{N}_2 p_s' = \underset{\sim}{Q}' \qquad (C.3)$$

$$\frac{\partial p_s}{\partial t} + \underset{\sim}{\nu}\cdot\underset{\sim}{D}' + Lp_s' + \underset{\sim}{N}_3\cdot\underset{\sim}{\psi}' = 0 \qquad (C.4)$$

and

$$f\underset{\sim}{\psi}' = \phi_s'\underset{\sim}{I} + \underset{\approx}{\gamma}\underset{\sim}{T}' + (\underset{\sim}{h}_1 + \underset{\sim}{h}_2)\,p_s' \qquad (C.5)$$

Here k is the zonal wavenumber of the perturbation, ϕ_s' and $\underset{\sim}{Q}'$ the complex amplitudes of the wavenumber k components of the surface geopotential and diabatic rate of change of temperature excluding Newtonian cooling, $\underset{\sim}{d}^c$ the Newtonian cooling rate and β the usual northward gradient of the coriolis parameter. $\underset{\approx}{\tau}$ and $\underset{\approx}{\nu}$ are also as given in Appendix B, and other matrices and vectors are given by

$$(\underset{\approx}{M}_1)_{\ell m} = \frac{ik}{f}\{\beta - k^2\overline{u}_\ell\}\delta_{\ell m},$$

$$(\underset{\approx}{M}_2)_{\ell m} = \frac{-iR}{k}\overline{p}_{sy}\left(\frac{1}{p}\frac{\partial p}{\partial p_s}\right)_\ell \delta_{\ell m},$$

$$(\underset{\sim}{N}_1)_\ell = \frac{iR}{k}\overline{T}_{y\ell}\left(\frac{1}{p}\frac{\partial p}{\partial p_s}\right)_\ell,$$

$$(\underset{\approx}{M}_3)_{\ell m} = ik\{\overline{T}_{y\ell}\delta_{\ell m} + \overline{p}_{sy}\left[\tau_{\ell m}\left(\frac{1}{\Delta p_m}\frac{\partial}{\partial p_s}\Delta p_m\right) - \kappa T_{r\ell}\left(\frac{1}{p}\frac{\partial p}{\partial p_s}\right)_\ell \delta_{\ell m}\right]\},$$

$$(\underset{\sim}{M}_4)_{\ell m} = (ik\bar{u}_\ell + d^c_\ell)\,\delta_{\ell m},$$

$$(\underset{\sim}{N}_2)_\ell = ik\{\sum_{m=1}^{NLEV}\left[\tau_{\ell m}\bar{u}_m\left(\frac{1}{\Delta p_m}\frac{\partial}{\partial p_s}\Delta p_m\right)\right] - \kappa T_{r\ell}\,\bar{u}_\ell\left(\frac{1}{p}\frac{\partial p}{\partial p_s}\right)_\ell\},$$

$$L = ik\sum_{\ell=1}^{NLEV}\nu_\ell\,\bar{u}_\ell\left(\frac{1}{\Delta p_\ell}\frac{\partial}{\partial p_s}\Delta p_\ell\right),$$

and

$$(\underset{\sim}{N}_3)_\ell = ik\,\bar{p}_{sy}\,\nu_\ell\left(\frac{1}{\Delta p_\ell}\frac{\partial}{\partial p_s}\Delta p_\ell\right)$$

We use $(\partial/\partial t)$ (C.5) together with (C.2), (C.3) and (C.4) to eliminate $\underset{\sim}{D}'$. (C.5) is then used to eliminate $\underset{\sim}{\psi}'$ from (C.3) and (C.4) . Defining the (NLEV+1) column vector $\underset{\sim}{e}$ by

$$(\underset{\sim}{e})_j = (\underset{\sim}{T}')_j \qquad , j \leq NLEV ,$$

$$= p_s \qquad , j = NLEV+1 ,$$

we then obtain an equation of the form

$$\frac{\partial \underset{\sim}{e}}{\partial t} + \underset{\approx}{M}\,\underset{\sim}{e} = \underset{\sim}{E}$$

Steady forced solutions are given by $\underset{\sim}{e} = (\underset{\approx}{M})^{-1}\,\underset{\sim}{E}$, and free normal mode solutions are obtained from the eigensolutions of $\underset{\sim}{M}$. The latter may also be used to produce time-dependent solutions for a transient forcing as described by Desmarais and Derome (1978).

The formulation and coding of the model has been tested by using high resolution to determine baroclinically-unstable solutions in the case of a uniform meridional temperature gradient. In this case the instability problem for the continuous model may be written analytically in terms of confluent hypergeometric functions (Charney, 1947), and readily solved numerically to arbitrary precision. Such calculations agree well with those obtained using the finite-difference model.

ECMWF PUBLISHED TECHNICAL REPORTS

No. 1 A Case Study of a Ten Day Prediction

No. 2 The Effect of Arithmetic Precisions on some Meteorological Integrations

No. 3 Mixed-Radix Fast Fourier Transforms without Reordering

No. 4 A Model for Medium-Range Weather Forecasting - Adiabatic Formulation

No. 5 A Study of some Parameterizations of Sub-Grid Processes in a Baroclinic Wave in a Two-Dimensional Model

No. 6 The ECMWF Analysis and Data Assimilation Scheme - Analysis of Mass and Wind Fields

No. 7 A Ten Day High Resolution Non-Adiabatic Spectral Integration: A Comparative Study

No. 8 On the Asymptotic Behaviour of Simple Stochastic-Dynamic Systems

No. 9 On Balance Requirements as Initial Conditions

No.10 ECMWF Model - Parameterization of Sub-Grid Processes

No.11 Normal Mode Initialization for a multi-level Gridpoint Model

No.12 Data Assimilation Experiments

No.13 Comparison of Medium Range Forecasts made with two Parameterization Schemes

No.14 On Initial Conditions for Non-Hydrostatic Models

No.15 Adiabatic Formulation and Organization of ECMWF's Spectral Model

No.16 Model Studies of a Developing Boundary Layer over the Ocean

No.17 The Response of a Global Barotropic Model to Forcing by Large-Scale Orography

No.18 Confidence Limits for Verification and Energetics Studies

No.19 A Low Order Barotropic Model on the Sphere with the Orographic and Newtonian Forcing

No.20 A Review of the Normal Mode Initialization Method

No.21 The Adjoint Equation Technique Applied to Meteorological Problems

No.22 The Use of Empirical Methods for Mesoscale Pressure Forecasts

No.23 Comparison of Medium Range Forecasts made with Models using Spectral or Finite Difference Techniques in the Horizontal

No.24 On the Average Errors of an Ensemble of Forecasts

No.25 On the Atmospheric Factors Affecting the Levantine Sea

No.26 Tropical Influences on Stationary Wave Motion in Middle and High Latitudes

ECMWF PUBLISHED TECHNICAL REPORTS

No.27 The Energy Budgets in North America, North Atlantic and Europe Based on ECMWF Analyses and Forecasts

No.28 An Energy and Angular-Momentum Conserving Vertical Finite-Difference Scheme, Hybrid Coordinates, and Medium-Range Weather Prediction